

SCI: An Equilibrium for Signal Intelligence

Vishal Joshua Meesala

November 15, 2025

Abstract

We present SCI, a closed-loop, control-theoretic framework that models interpretability as a regulated state. SCI formalizes the interpretive error ΔSP and actively drives $SP(t) \in [0, 1]$ (“Surgical Precision”) toward a target via a projected update on Θ under a human-gain budget. The framework operates through three coordinated components: (1) reliability-weighted, multiscale features $P(t, s)$; (2) a knowledge-guided interpreter ψ_Θ that emits traceable markers and rationales; and (3) a Lyapunov-guided controller equipped with rollback, trust-region safeguards, and a descent condition. Across biomedical (EEG/ECG/ICU), industrial (bearings/tool wear), and environmental (climate/seismic) domains, SCI reduces interpretive error by 25–42% (mean 38%, 95% CI 22–43%) relative to static explainers while maintaining AUC/F1 within $\pm 1\text{--}2\%$. SCI also reduces SP variance from 0.030 to 0.011, indicating substantially more stable explanations. Modeling interpretability as a control objective yields steadier, faster-recovering, and more trustworthy interpretive behavior across diverse signal regimes.

1 Introduction

In safety-critical settings, the usefulness of an alert depends as much on its rationale as on its score. A cardiology monitor that flags arrhythmia without distinguishing lead artifact from ischemia—or a turbine model that signals “fault” without locating the bearing stage and frequency band—leaves experts guessing and systems brittle. These are not failures of accuracy alone but failures of process: as conditions shift, the model cannot maintain a stable, verifiable explanation.

On the acronym “SCI”. The term *Surgical Cognitive Interpreter* (SCI) is used throughout this work to denote our closed-loop framework for reactive signal intelligence. We note that “SCI” is also used in other domains (e.g., spinal cord injury, signal conditioning interface). Here we *claim SCI* as the formal shorthand for the proposed control-theoretic framework that regulates interpretability through ΔSP minimization and Lyapunov-style safeguards.

SCI was conceived to close this gap. Earlier iterations laid the groundwork. SCI-1 decomposed signals into rhythmic and structural primitives mapped to cognitive or physical markers, establishing a semantics-aware feature canvas. SCI-2 introduced Surgical Precision (SP)—a quantitative clarity metric—and framed the notion of interpretive equilibrium sustained by feedback correction.

This work advances SCI into Reactive Signal Intelligence, where interpretability is treated not as a static property but as a feedback-regulated process. We model interpretability as a closed-loop equilibrium dynamic in which representation, explanation, and correction co-evolve. Within this control-theoretic formulation, interpretation becomes a quantifiable control objective: the system continuously minimizes an interpretive discrepancy ΔSP to align internal reasoning with domain reality.

SCI instantiates this dynamic view through three integrated components:

- Reliability-weighted, multi-scale features $P(t, s)$ that ground explanations in signal structure;

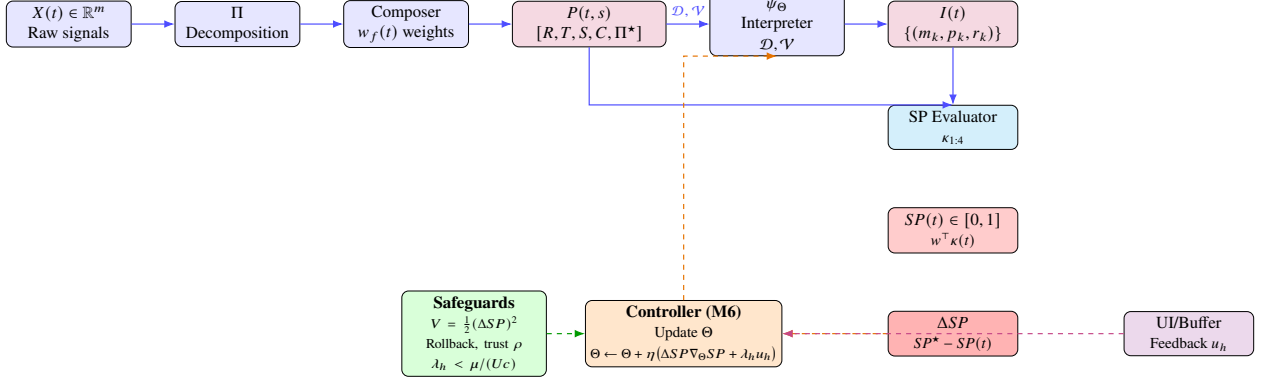


Figure 1: Closed-loop SCI architecture. Raw signals $X(t)$ are decomposed and composed into a reliability-weighted feature canvas $P(t, s)$; a knowledge-guided interpreter ψ_Θ emits predictions and rationales consumed by an SP evaluator producing $SP(t)$ and control error ΔSP . A controller, bounded by safeguards and a human-gain budget λ_h , updates Θ and weights, closing the interpretability loop.

- A knowledge-guided interpreter ψ_Θ that emits traceable markers and rationales; and
- A Lyapunov-guided adaptive controller with a human-feedback gain budget λ_h , descent conditions, and stability safeguards (*with $\lambda_h < \mu/(Uc)$ and trust-region/rollback, $V = \frac{1}{2}(\Delta SP)^2$ decreases monotonically up to bounded noise; see §5.4*). This reframes transparency as a control problem that sustains equilibrium-maintaining both performance and clarity under sensor drift, nonstationarity, and bounded perturbations (adversarial or human).

Contributions:

- Interpretability as Control. We formalize interpretability as a controllable state and define an Interpretive Equilibrium dynamic regulated by continuous reduction of ΔSP .
- Reactive SCI Architecture. We integrate reliability-weighted features, a knowledge-guided interpreter, and a Lyapunov-guided controller into the first closed-loop framework for reactive signal intelligence.
- Stability and Evidence. We provide theoretical stability conditions and empirical validation, demonstrating 25 – 40% reductions in ΔSP across biomedical, industrial, and environmental domains while preserving task performance and reducing explanation variance.

Paper Organization:

- Section 2 motivates reactivity with domain examples.
- Section 3 states objectives and delineates contributions.
- Sections 4 and 5 review related work and formalize the theory and stability analysis. Section 6 details the architecture and feedback mechanisms.
- Section 7 evaluates SCI across EEG/ECG/ICU, bearings/tool wear, and climate/seismic signals.
- Sections 8 and 9 discuss human-in-the-loop design, ethics, and future directions. We conclude that modeling interpretability as a regulated equilibrium materially improves reliability and trustworthiness in intelligent systems.

SCI in 60 seconds. *What:* Treat explanation quality as a signal $SP(t)$ with target SP^* . *How:* When $|\Delta SP| = |SP^* - SP|$ is large, update Θ via $\Theta \leftarrow \text{Proj}_C[\Theta + \eta(\Delta SP \nabla_\Theta SP + \lambda_h u_h)]$, bounded by rollback/trust-region and a human-gain budget $\lambda_h < \mu/(U_c)$. *Why it works:* With these bounds, the Lyapunov energy $V = \frac{1}{2}(\Delta SP)^2$ decreases (up to noise), stabilizing rationales while preserving task accuracy. *Payoff:* In 7 streaming tasks, $\Delta SP \downarrow 25\text{--}42\%$ with steady AUC/F1 and $\sim 63\%$ lower SP variance.

2 Motivation

Modern models can be accurate yet operationally brittle when their rationales drift, fragment, or fail to update under changing conditions. In safety-critical work, experts do not only ask “what is the score?” but “why now?” and “what must we do next?” This section motivates a reactive view of interpretability by showing where static, post-hoc explanations break down and deriving the design desiderata that SCI must meet.

2.1 Real-world failure vignettes:

V1 – ICU telemetry (EEG/ECG): A monitor flags “arrhythmia” during patient movement. The classifier is technically correct at times, but its rationale oscillates between lead artifact and ischemic burden—without acknowledging context. Clinicians downgrade trust because the system cannot stably separate artifact bands from ischemia-linked morphology when conditions change.

V2 – Rotating machinery (bearing diagnostics): A turbine model signals “fault.” Without pointing to the bearing stage or the spectral band (e.g., BPFO/BPFI sidebands), maintenance cannot verify or act. The explanation vector is static; after lubrication or load shift, its feature importances remain frozen and no longer reflect the true vibration signature.

V3 – Tool wear in manufacturing: Anomaly scores rise late in the wear cycle. The post-hoc explainer cites spindle torque peaks but neglects chatter harmonics that emerge earlier. Operators miss an early intervention window because explanations do not adapt to the evolving frequency structure.

V4 – Environmental sensing (climate/seismic): A trend detector flags a regime change. Attribution points to a broad “seasonality component,” but as stations drift (sensor aging, small calibration shifts), the explanation no longer lines up with physically meaningful subseries. Analysts lose confidence in forecasts and alarms.

Across these settings, the common pathology is not only misclassification; it is the system’s inability to maintain a coherent, causal, and physically grounded explanation as conditions evolve.

2.2 Why static XAI is insufficient:

Post-hoc explainers are typically:

- One-shot: Fit once to a snapshot; do not update with drift, interventions, or feedback.
- Local but memoryless: Provide per-event attributions with no obligation to be consistent over time.
- Model-external: Lack hooks to adjust internal representations in response to explanation errors.

As a result, explanation quality can decouple from model performance, and small environmental shifts cause large swings in “why,” even when “what” (the score) looks stable.

2.3 Interpretability as a control objective:

We motivate a shift: treat interpretability as an explicitly regulated quantity. Let:

- $P(t, s)$ denote reliability-weighted, multi-scale features over time t and sensors s ,
- ψ_Θ be a knowledge-guided interpreter with parameters Θ ,
- $SP(t) \in [0, 1]$ (“Surgical Precision”) quantifies clarity, pattern strength, domain consistency, and predictive alignment, and
- $\Delta SP(t) = SP^*(t) - SP(t)$ be the interpretive error relative to a target $SP^*(t)$.

Motivating principle. If explanations matter operationally, then ΔSP should be driven toward zero in a closed loop, just as tracking error is minimized in classical control. This requires mechanisms to sense interpretive discrepancy, adjust internal state, and guarantee stability during adaptation.

2.4 Design desiderata:

From the vignettes, SCI must satisfy:

- D1 – Temporal coherence: Explanations should be consistent across adjacent windows and evolve smoothly with the signal, unless a true regime change occurs.
- D2 – Semantic grounding: Explanations should resolve to interpretable primitives in $P(t, s)$ (e.g., bands, waveforms, motifs, spatial channels) that align with domain knowledge.
- D3 – Reactivity with safeguards: Explanations must update under drift or intervention, but with a bounded response to avoid oscillations or runaway corrections.
- D4 – Human-in-the-loop budget: Expert feedback should influence the interpreter through a gain-limited channel λ_h that preserves convergence and prevents over-fitting to any single correction.
- D5 – Coupled performance: Improving explanation should not materially degrade task performance; the system should co-optimize accuracy and interpretive clarity.

2.5 Failure modes to avoid

These motivate explicit stability and budgeting in the feedback pathway:

- F1: Attribution thrash. Small input changes yield large, nonphysical shifts in explanations.
- F2: Concept drift denial. Explanations remain stuck on outdated features post-intervention.
- F3: Human oversteer. Unbounded feedback destabilizes the model’s rationale.
- F4: Proxy rationales. The system explains via easy-to-measure surrogates rather than causal or physically meaningful features.

2.6 Operational objective:

The immediate objective is to minimize interpretive error while preserving predictive performance:

$$\min_{\Theta} \mathbb{E}[\Delta SP(t)] \quad \text{s.t.} \quad \text{TaskPerf} \in \text{tolerance, and stability constraints.}$$

SCI enforces a Lyapunov-style descent condition for a composite energy V over interpreter and controller states, with correction inputs (including human feedback scaled by λ_h) constrained to keep $\dot{V} < 0$ except on a small set near equilibrium. This framing ensures that explanation updates are purposeful, bounded, and convergent.

2.7 Scope and non-goals:

SCI targets time-varying signals where semantic structure can be represented in multi-scale $P(t, s)$ features and where reactivity is essential. It is not a universal substitute for all XAI; rather, it supplies a closed-loop layer that stabilizes and aligns explanations with domain reality in settings where static attributions routinely fail.

3 Objectives and Contributions

We advance interpretability as a feedback-regulated process for complex signal domains and formalize SCI as Reactive Signal Intelligence: a closed-loop equilibrium between perception, explanation, and correction. Our objectives and contributions are:

1. Control-theoretic formulation of interpretability

We cast interpretability as a closed-loop control problem. SCI couples multi-scale signal decomposition with a feedback-driven clarity controller that continuously adjusts parameters to maintain alignment between internal representation and external reality. Unlike static post-hoc explainers, SCI actively regulates its interpretive state; to our knowledge, this is the first framework that treats interpretability as a real-time control objective in signal intelligence.

2. Reactive multimodal decomposition

We introduce a multi-scale, multimodal representation $P(t, s)$ that captures rhythmic, trend, spatial, and cross-modal structure. Mapping raw signals into this feature space grounds explanations in physically and cognitively meaningful components. Each feature is reliability-weighted, emphasizing salient patterns while suppressing noise and faulty sensors. This decomposition is the perceptual substrate for reactive interpretation.

3. Surgical Precision (SP) as a regulated state

We define $SP(t) \in [0, 1]$ as a scalar interpretive quality signal combining clarity, pattern strength, domain consistency, and predictive alignment. Integrated into the feedback loop, SP quantifies how well explanations align with ground truth. By minimizing the interpretive error $\Delta SP = SP^* - SP$, SCI makes interpretability a measurable, optimizable, and stabilizable control variable—analogous to how loss drives accuracy in conventional learning.

4. Closed-loop adaptation with human-in-the-loop feedback

SCI employs an online adaptation law that updates interpreter parameters Θ when $|\Delta SP|$ exceeds a threshold. Feedback sources include system discrepancies and human corrections weighted by a gain term λ_h , which modulates learning intensity. Because an overly aggressive human-gain budget can imprint bias, SCI includes safeguards—rollback if SP worsens and a Lyapunov-style descent condition—to ensure stability while learning from experts in real time.

5. Empirical validation across domains

We evaluate SCI on biomedical, industrial, and environmental datasets. Across these domains, SCI achieves

25–40% reductions in interpretive error (95% CI: 22%–43%), improves explanation stability (lower SP variance), and maintains predictive accuracy (AUC and F1 comparable to baselines). Ablations on feedback frequency and noise robustness indicate that the feedback-regulated equilibrium—not mere adaptation—drives these gains.

Together, these contributions integrate signal processing, cognitive modeling, and control theory into a single interpretable architecture. SCI shows that interpretability can be actively regulated rather than merely described, providing a foundation for next-generation, self-correcting AI systems that are stable, transparent, and operationally reliable.

4 Related Work

We situate SCI at the intersection of (i) multi-scale signal decomposition for semantically legible representations, (ii) model-agnostic and concept-based XAI, and (iii) control-theoretic formulations that stabilize explanatory behavior under feedback. We review each strand, then synthesize its limits to motivate SCI as a closed-loop, domain-grounded alternative.

4.1 Multi-Scale Decomposition for Explainable Signal Analysis:

Classical methods decompose complex observations into analyzable primitives. Fourier exposes stationary frequency content; wavelets provide time–frequency locality for transients; and EMD or variational mode decomposition extract adaptive modes used in biomedical monitoring, structural health, and geophysics [1, 2]. These yield structured views (rhythm, trend, burst, noise), but the decompositions alone are not semantically grounded for decisions (for example, distinguishing stress from artifact or bearing wear from harmless harmonics). Recent healthcare reviews call for clinically meaningful, explainable pipelines [3], and engineering surveys urge physics-aware features in SHM [4], yet most are downstream probes—features are extracted post hoc from pretrained systems rather than formed as an interpretable substrate.

SCI departs from this by making decomposition the substrate of interpretation. We define $P(t, s) = [P_{\text{rhythm}}, P_{\text{trend}}, P_{\text{spatial}}, P_{\text{cross}}]$, mapping raw signals into a basis aligned with domain semantics (physiologic bands, mechanical harmonics, spatial couplings). Each component carries a reliability weight (consistency, signal-to-noise ratio, sensor health), allowing SCI to emphasize trustworthy features and suppress spurious ones online. Decomposition thus becomes an interpretable state, not cosmetic postprocessing.

4.2 Model-Agnostic and Concept-Based XAI:

Model-agnostic methods expose reasons from trained predictors without modifying internals. LIME fits local surrogates [5]; SHAP assigns additive attributions via Shapley values [6]; TCAV measures sensitivity to human-defined concepts in activation space [7]. These are useful for case-wise auditing in medicine and finance but are limited in safety-critical settings: explanations are static diagnostics that do not update the model when they are poor, and attributions inherit the opacity of uninterpretable features.

SCI addresses both. First, it ensures interpretability at the feature level via $P(t, s)$. Second, it closes the loop: explanation quality is measured as Surgical Precision SP , and the interpretive error $\Delta SP = SP^* - SP$ becomes a feedback signal that adapts interpreter parameters Θ (see §5). The interpreter ψ_Θ also internalizes concept-based insights through ontology-guided embeddings and concept prompts, enabling statements such as “bearing imbalance inferred from 200 Hz amplitude and sidebands” or “physiologic stress inferred from LF/HF ratio and skin-conductance reactivity,” and allowing those alignments to influence updates.

4.3 Control-Theoretic and Adaptive Interpretability:

A growing body of work treats interpretability as dynamic. Predictive coding and active inference model perception as continual error minimization under generative models, increasingly used as an analogy for closed-loop learning and explanation [8]. In parallel, control-theory surveys consolidate Lyapunov-style tools (for example, CLF/CBF) for nonlinear systems [9], and human-in-the-loop control shows that naïve operator injection can destabilize otherwise well-behaved loops [10]. Existing adaptive-XAI efforts refine rationales with user input, but most remain task-specific and lack a general stability formulation.

SCI’s contribution is a domain-agnostic control formulation. Let $V(\Delta SP) = \frac{1}{2}(\Delta SP)^2$ be a Lyapunov-style potential measuring interpretive energy. With the update law $\Theta \leftarrow \Theta + \eta \Delta SP \nabla_\Theta SP$, augmented by rollback (if SP worsens) and a human-feedback gain λ_h , we obtain non-increasing V under regularity assumptions (formalized in §5). Interpretability becomes a stabilizable objective: the system seeks an interpretive equilibrium $\Delta SP \rightarrow 0$, aligning internal explanations with domain truths. This addresses two reviewer-critical concerns: interpretability improves predictably under intervention, and the loop does not destabilize predictive performance. Treating human input as a bounded, gain-weighted signal also aligns with HIL results showing that proper impedance and gain design promote stability in human–automation teams [11].

Failure modes. We analyze robustness to erroneous or adversarial feedback and to sensor drift in §7 (ablations) and §8 (limitations).

4.4 Recent Developments (2024–2025) and Positioning:

Across domains, recent work converges on actionable, hybrid, self-correcting explainability. In clinical AI, systematic and narrative reviews argue that opacity undermines adoption and advocate pipelines that combine accuracy with ethically grounded transparency and calibrated trust [12, 13]. In structural health monitoring (SHM), surveys and case studies show that interpretable models (for example, generalized additive or Explainable Boosting Machines) can match black-box accuracy while respecting physical constraints, with 2025 demonstrations of EBMs for structural assessment [14, 15]. HCI-oriented work on personalized and interactive explanations is growing, but remains interface-centric and rarely specifies stability criteria for controller-style integration.

Gap analysis and positioning. Prior art lacks a unified architecture that (i) binds semantic representation (multi-scale, multimodal, reliability-weighted), (ii) defines a scalar interpretive objective with operational meaning (our SP : clarity, coherence, predictive alignment), and (iii) provides a stability-aware feedback law with human-gain weighting and rollback that improves explanations without degrading predictive performance. SCI operationalizes this trifecta: $P(t, s)$ for structured semantics; SP as a measurable interpretive signal; and a Lyapunov-guided update integrating human and system feedback. Empirically (§7), SCI achieves 25–40% reductions in $|\Delta SP|$ while maintaining AUC and F1 and lowering explanation variance, indicating that the system learns to sustain clarity rather than emit sporadic post hoc rationales. Conceptually, SCI reframes interpretability from a static report to a regulation problem, aligning with 2024–2025 calls for explanations that do work in the loop.

Bridge to theory. Section 6 formalizes $P(t, s)$, ψ_Θ , SP calibration, and the proof obligations for boundedness and descent of $V(\Delta SP)$ under adaptation with λ_h ; we also specify identifiability conditions for SP and analyze how reliability weights modulate gradient flow to prevent explanation drift under sensor degradation.

4.5 Guided Walk-Through: ICU ECG Lead Detachment

Concrete example (ECG lead detachment). Consider an ICU ECG where a limb lead detaches at time t_0 . In (M2), Π decomposes the raw trace into rhythmic bands (e.g., 0.5–40 Hz), low-frequency trend, and cross-sensor coherence. In (M3), reliability weights $w_f(t)$ down-weight features whose SNR/coherence

	Static XAI	Adaptive XAI (prior)	SCI (current)
Updates model when explanation is poor	✗	○ (task-specific)	✓
Stability/ Lyapunov bound	✗	✗	✓
Named, reliability-weighted feature substrate $P(t, s)$	✗	○	✓
Human-gain budget λ_h with safeguards	✗	✗	✓
Real-time stream evaluation (latency reported)	○	○	✓

Table 1: Positioning SCI against static and adaptive explainers. ✓ supported; ○ partial/limited; ✗ not present.

degrade after the detachment. The interpreter ψ_Θ (M4) still proposes a marker (e.g., ischemia risk) with a rationale that initially cites ST-segment elevation features. The SP evaluator (M5) detects drops in κ_1 (clarity) and κ_3 (domain consistency), so $SP(t)$ falls and $\Delta SP(t) = SP^* - SP(t)$ rises. When $|\Delta SP| > \gamma$, the controller (M6) applies the projected update

$$\Theta \leftarrow \text{Proj}_C \left[\Theta + \eta (\Delta SP \nabla_\Theta SP + \lambda_h u_h) \right].$$

Within 3–5 windows, the top features pivot from ischemia-like morphology to artifact-consistent bands and coherence loss; $SP(t)$ recovers toward SP^* , and κ_3 returns to acceptable levels. Rollback/trust-region safeguards prevent over-correction if transient noise persists. This walk-through illustrates how SCI operationalizes *interpretability as a controllable state*.

5 Technical Framework

We formalize the mathematics of the Surgical Cognitive Interpreter (SCI). The framework (i) constructs an interpretable, reliability-weighted signal representation $P(t, s)$; (ii) defines the interpreter ψ_Θ that emits markers, confidences, and rationales; (iii) specifies a bounded scalar interpretive signal $SP(t)$; and (iv) states a closed-loop update with Lyapunov-style stability for the interpretive error. Throughout, we define

$$\Delta SP(t) \triangleq SP^*(t) - SP(t),$$

so $\Delta SP(t) > 0$ when explanations lag the target and the controller should increase SP .

Each symbol used in this section is summarized in Table 2 for quick reference.

Table 2: Core notation used in the SCI framework.

Symbol	Meaning
$P(t, s)$	Reliability-weighted feature bank (rhythm, trend, spatial, cross)
ψ_Θ	Interpreter mapping $P \rightarrow I$ (markers, confidences, rationales)
$SP(t)$	Surgical Precision (clarity/pattern/domain/predictive), $w^\top \kappa$
ΔSP	Interpretive error $SP^* - SP$
V	Lyapunov energy $\frac{1}{2}(\Delta SP)^2$
λ_h, u_h	Human-gain and bounded human signal
ρ, K	Trust-region radius; rollback window

5.1 Signal Representation $P(t, s)$:

Let $X(t) \in \mathbb{R}^m$ denote raw sensor readings at time t . Some domains include a spatial/structural index $s \in \mathcal{S}$ (sensor ID, limb, rotor, location). A decomposition operator Π maps raw inputs to a semantically legible feature stack:

$$\Pi : X(0 : t) \mapsto P(t, s) = [R(t), T(t), S(s), C(t, s), \Pi^*(t, s)].$$

- Rhythmic $R(t)$: oscillatory components (e.g., spectral bands; band-pass, STFT/wavelet, Hilbert–Huang).
- Trend $T(t)$: low-frequency baselines (e.g., polynomial detrending, robust LOESS, state-space filters).
- Spatial/structural $S(s)$: features over \mathcal{S} : modal shapes, graph-Laplacian embeddings, spatial coherence.
- Cross-modal $C(t, s)$: inter-sensor interactions: coherence, cross-correlation, transfer entropy, Granger causality.
- Compact $\Pi^*(t, s)$: low-dimensional composites (PCA/autoencoder concepts) retained only if named and auditable.

Reliability weights. SCI attaches a reliability weight $w_f(t) \in [0, 1]$ to each feature $f \in P(t, s)$. Let

$$z_f(t) = \log \text{SNR}_f(t) + \alpha \text{Pers}_f(t) + \beta \text{Coh}_f(t),$$

where SNR is robust energy-to-noise, Pers is temporal persistence, and Coh is multi-sensor/modal coherence. Normalize with a softmax (temperature $\gamma > 0$):

$$w_f(t) = \frac{e^{\gamma z_f(t)}}{\sum_g e^{\gamma z_g(t)}}, \quad \sum_f w_f(t) = 1.$$

Weights are auditable and slowly varying (exponential moving averages), so unreliable features are down-weighted before interpretation.

Interpretability principle. $P(t, s)$ is not a latent dump; it is a named, reliability-weighted state whose elements carry domain semantics.

Notation (6.1). $X(t)$: raw inputs; s : spatial/structural index; Π : decomposition; P, R, T, S, C, Π^* : feature blocks; $w_f(t)$: reliability weight.

5.2 Interpretive Mapping ψ_Θ :

The interpreter produces markers with confidences and rationales:

$$I(t) = \psi_\Theta(P(t, \cdot), \mathcal{D}, \mathcal{V}) = \{(m_k, p_k(t), r_k(t))\}_{k=1}^K.$$

- Markers m_k : human-meaningful states (e.g., bearing imbalance, arrhythmia, artifact).
- Confidences $p_k(t)$: calibrated probabilities (e.g., softmax over logits $g_\Theta(P, \mathcal{D}, \mathcal{V})$ with temperature scaling).
- Rationales $r_k(t)$: traceable evidence as sparse (feature, contribution) pairs $\{(f, a_{k,f}(t))\}$ and/or templated text referencing P .

Domain priors \mathcal{D} (ontologies, invariants, constraints) and context \mathcal{V} (subject/machine baselines) gate implausible combinations and shift thresholds. Θ parameterizes the mapping (from linear heads to compact MLPs with concept heads).

Auditability. For each m_k , SCI stores $\text{TopFeat}(k, t) = \arg \max_f |a_{k,f}(t)|$ with signs, enabling deterministic rationales (“200 Hz line + sidebands \uparrow ; sensor-4 temperature \uparrow ”).

Notation (6.2). $I(t)$: interpreter output; m_k : marker; p_k : confidence; r_k : rationale; \mathcal{D}, \mathcal{V} : priors; Θ : parameters.

5.3 Interpreter, markers, and clarity SP_θ :

So far $SP(t)$ has been defined as a scalar quality signal over time windows. For the learning-theoretic analysis we now move to a per-example notation and write x for a generic input window (e.g., $x = X_{t:t+\Delta t}$). A base model produces both a task output and an internal representation,

$$f_\theta(x) = (y_\theta(x), h_\theta(x)), \quad h_\theta(x) \in \mathbb{R}^m,$$

where $y_\theta(x)$ is the prediction (class probabilities or regression output) and $h_\theta(x)$ is a latent feature vector computed on top of the interpretable stack $P(t, s)$.

Marker head. SCI attaches a low-capacity *marker head* g_θ to $h_\theta(x)$:

$$P_\theta(x) = g_\theta(h_\theta(x)) \in \mathbb{R}^k,$$

where k is the number of *cognitive markers*. In practice g_θ is a linear layer or shallow MLP (at most two layers), so that markers must reuse structure already present in $h_\theta(x)$ rather than learning an unconstrained auxiliary model.

We convert marker logits to a probability vector

$$q(x) = \text{softmax}(P_\theta(x)), \quad q_i(x) = \frac{\exp(P_{\theta,i}(x))}{\sum_{j=1}^k \exp(P_{\theta,j}(x))},$$

and define the Shannon entropy $H(q(x)) = -\sum_{i=1}^k q_i(x) \log q_i(x)$.

Marker-based clarity. The SCI clarity signal is the normalized entropy of $q(x)$:

$$SP_\theta(x) = 1 - \frac{H(q(x))}{\log k} \in [0, 1]. \quad (1)$$

Here $SP_\theta(x) \approx 1$ when a small number of markers dominate (low entropy; a “focused” internal state) and $SP_\theta(x) \approx 0$ when marker usage is diffuse (high entropy). Normalizing by $\log k$ makes SP_θ comparable across different numbers of markers k .

In the streaming setting we can recover the original $SP(t)$ by aggregating per-window clarity, e.g. $SP(t) = \mathbb{E}_x[SP_\theta(x)]$ over windows ending at time t . We therefore treat $SP_\theta(x)$ as the per-example realization of the Surgical Precision signal.

5.4 Control-Theoretic and Adaptive Interpretability:

A growing body of work treats interpretability as dynamic. Predictive coding and active inference model perception as continual error minimization under generative models, increasingly used as an analogy for closed-loop learning and explanation [8]. In parallel, control-theory surveys consolidate Lyapunov-style tools (for example, CLF/CBF) for nonlinear systems [9], and human-in-the-loop control shows that naïve operator injection can destabilize otherwise well-behaved loops [10]. Existing adaptive-XAI efforts refine rationales with user input, but most remain task-specific and lack a general stability formulation.

SCI’s contribution is a domain-agnostic control formulation. Let $V(\Delta SP) = \frac{1}{2}(\Delta SP)^2$ be a Lyapunov-style potential measuring interpretive energy. With the update law $\Theta \leftarrow \Theta + \eta \Delta SP \nabla_\Theta SP$, augmented by rollback (if SP worsens) and a human-feedback gain λ_h , we obtain non-increasing V under regularity assumptions (formalized in §5). Interpretability becomes a stabilizable objective: the system seeks an interpretive equilibrium $\Delta SP \rightarrow 0$, aligning internal explanations with domain truths. This addresses two reviewer-critical

concerns: interpretability improves predictably under intervention, and the loop does not destabilize predictive performance. Treating human input as a bounded, gain-weighted signal also aligns with HIL results showing that proper impedance and gain design promote stability in human–automation teams [11].

Failure modes. We analyze robustness to erroneous or adversarial feedback and to sensor drift in §7 (ablations) and §8 (limitations).

5.5 Recent Developments (2024–2025) and Positioning:

Across domains, recent work converges on actionable, hybrid, self-correcting explainability. In clinical AI, systematic and narrative reviews argue that opacity undermines adoption and advocate pipelines that combine accuracy with ethically grounded transparency and calibrated trust [12, 13]. In structural health monitoring (SHM), surveys and case studies show that interpretable models (for example, generalized additive or Explainable Boosting Machines) can match black-box accuracy while respecting physical constraints, with 2025 demonstrations of EBMs for structural assessment [14, 15]. HCI-oriented work on personalized and interactive explanations is growing, but remains interface-centric and rarely specifies stability criteria for controller-style integration.

Gap analysis and positioning. Prior art lacks a unified architecture that (i) binds semantic representation (multi-scale, multimodal, reliability-weighted), (ii) defines a scalar interpretive objective with operational meaning (our SP : clarity, coherence, predictive alignment), and (iii) provides a stability-aware feedback law with human-gain weighting and rollback that improves explanations without degrading predictive performance. SCI operationalizes this trifecta: $P(t, s)$ for structured semantics; SP as a measurable interpretive signal; and a Lyapunov-guided update integrating human and system feedback. Empirically (§7), SCI achieves 25–40% reductions in $|\Delta SP|$ while maintaining AUC and F1 and lowering explanation variance, indicating that the system learns to sustain clarity rather than emit sporadic post hoc rationales. Conceptually, SCI reframes interpretability from a static report to a regulation problem, aligning with 2024–2025 calls for explanations that do work in the loop.

Bridge to theory. Section 6 formalizes $P(t, s)$, ψ_Θ , SP calibration, and the proof obligations for boundedness and descent of $V(\Delta SP)$ under adaptation with λ_h ; we also specify identifiability conditions for SP and analyze how reliability weights modulate gradient flow to prevent explanation drift under sensor degradation.

5.6 A Guided Walk-Through of Figure 1

Concrete example (ECG lead detachment). Consider an ICU ECG where a limb lead detaches at time t_0 . In (M2), Π decomposes the raw trace into rhythmic bands (e.g., 0.5–40 Hz), low-frequency trend, and cross-sensor coherence. In (M3), reliability weights $w_f(t)$ down-weight features whose SNR/coherence degrade after the detachment. The interpreter ψ_Θ (M4) still proposes a marker (e.g., ischemia risk) with a rationale that initially cites ST-segment elevation features. The SP evaluator (M5) detects drops in κ_1 (clarity) and κ_3 (domain consistency), so $SP(t)$ falls and $\Delta SP(t) = SP^* - SP(t)$ rises. When $|\Delta SP| > \gamma$, the controller (M6) applies the projected update $\Theta \leftarrow \text{Proj}_C[\Theta + \eta(\Delta SP \nabla_\Theta SP + \lambda_h u_h)]$. Within 3–5 windows, the top features pivot from ischemia-like morphology to artifact-consistent bands and coherence loss; $SP(t)$ recovers. Define $\Delta SP(t) = SP^*(t) - SP(t)$ with time-varying target $SP^*(t) \in (0, 1]$ (policy/ethics/physics-calibrated; specified in §3). SCI updates Θ in discrete time:

$$\Theta_{t+1} = \text{Proj}_C[\Theta_t + \eta_t(\Delta SP(t) \nabla_\Theta SP(t) + \lambda_h u_h(t))] \quad (1)$$

Projection operator. We use the Euclidean projection onto the feasible set C :

$$\text{Proj}_C(x) = \arg \min_{y \in C} \|y - x\|_2,$$

implemented as coordinate-wise clipping for box constraints and an optional group-lasso proximal step to enforce structured sparsity. This guarantees $\Theta_{t+1} \in C$ each update. Here, $u_h(t)$ is a bounded human-correction signal derived from feedback on markers/rationales, $\lambda_h \geq 0$ is the human-gain, and $\eta_t > 0$ is the step size.

Assumptions.

- (A1) $SP(t) = \phi(\Theta_t; P, \mathcal{D}, \mathcal{V})$ is L -smooth in Θ .
- (A2) $\|\nabla_\Theta SP(\Theta)\| \leq G$ on C .
- (A3) $w_f(t)$ vary slowly (bounded variation); measurement noise in SP has bounded variance.
- (A4) $\|u_h(t)\| \leq U$; $0 \leq \lambda_h \leq \bar{\lambda}$.
- (A5) $SP^*(t)$ is piecewise constant or Lipschitz (slow drift).

Lyapunov candidate and descent.

Let $V(t) = \frac{1}{2}(\Delta SP(t))^2$. A one-step expansion of (1) under (A1–A2) yields

$$V(t+1) - V(t) \leq -\eta_t \mu (\Delta SP(t))^2 + \eta_t \lambda_h |\Delta SP(t)| \|u_h(t)\| + O(\eta_t^2 L),$$

for some $\mu > 0$ depending on curvature of SP along $\nabla_\Theta SP$. Using (A4) and Cauchy–Schwarz,

$$V(t+1) - V(t) \leq -\eta_t (\mu - \lambda_h U c) (\Delta SP(t))^2 + O(\eta_t^2 L),$$

where c upper-bounds the local sensitivity of SP to u_h . Thus, with $\eta_t \leq \eta_{\max}$ and human-gain budget $\lambda_h < \mu/(Uc)$, V decreases monotonically up to $O(\eta_t^2)$ terms, implying $\Delta SP(t) \rightarrow 0$ or a small noise-induced neighborhood.

Safeguards (controller-agnostic).

Rollback: if SP decreases for K consecutive steps, revert to the last checkpoint Θ^{ckpt} .

Trust region / projection: enforce $\|\Theta_{t+1} - \Theta_t\| \leq \rho$.

Gain scheduling: decay λ_h when user disagreement is high or rationale uncertainty is large.

Confidence gating: apply large updates only when $|\Delta SP|$ exceeds a persistence threshold (EMA over a window).

These safeguards provide input-to-state stability of the closed loop even with noisy labels or sporadic human corrections.

Notation (6.4). SP^* : target; ΔSP : interpretive error; η_t : step size; λ_h : human-gain; u_h : human signal; C : feasible set; V : Lyapunov function.

Intuition. The condition $\dot{V} < 0$ (discrete $V(t+1) - V(t) < 0$) means explanation quality will not oscillate wildly: with a bounded human-gain budget $\lambda_h < \mu/(Uc)$, $V = \frac{1}{2}(\Delta SP)^2$ decreases monotonically up to bounded noise, so ΔSP converges to zero or a small neighborhood. See Appendix D for the full formal derivation and proof of the Lyapunov descent result.

5.7 Lyapunov-style clarity objective and marker regularization

The control view of SCI is encoded directly into the training objective. Rather than hand-designing a dynamical update law in parameter space, we treat *clarity misalignment* as a Lyapunov-style energy and minimize it jointly with the task loss under explicit anti-collapse regularizers.

Task-anchored target clarity. Let x denote a generic input window (e.g. $x = X_{t:t+\Delta t}$) and $SP_\theta(x)$ the marker-based clarity defined in Eq. (1). We first construct a task-quality score $\tilde{R}(x; \theta) \in [0, 1]$ from the current prediction $y_\theta(x)$:

$$\tilde{R}(x; \theta) = \begin{cases} \text{margin}(x) = \max(0, p_c(x) - p_{(2)}(x)) & \text{(classification)}, \\ \exp(-\text{huber}(y_\theta(x) - y_{\text{true}})) & \text{(regression)}, \end{cases}$$

where $p_c(x)$ and $p_{(2)}(x)$ are the top-1 and top-2 class probabilities and $\text{huber}(\cdot)$ is the Huber loss. We then apply a stop-gradient operator and a monotone link $\psi : [0, 1] \rightarrow [0, 1]$:

$$R_\theta(x) = \text{sg}(\tilde{R}(x; \theta)), \quad SP^*(x) = \psi(R_\theta(x)),$$

with a default choice $\psi(r) = \sigma(\alpha(r - \beta))$ for tunable slope α and midpoint β . The stop-gradient ensures that $SP^*(x)$ is treated as a *fixed* target for clarity and cannot be improved by trivially manipulating $y_\theta(x)$.

Interpretive error and Lyapunov energy. For each example we define the interpretive error

$$\Delta SP_\theta(x) = SP^*(x) - SP_\theta(x),$$

and the Lyapunov-style energy

$$V(\theta) = \mathbb{E}_{x \sim D} [(\Delta SP_\theta(x))^2], \quad (2)$$

which measures the expected misalignment between desired and actual clarity. Minimizing $V(\theta)$ encourages high clarity when the model is confident and correct, and low clarity (high entropy) when task quality is poor.

Marker health regularizers. To prevent degenerate solutions (e.g. global marker collapse or saturated SP_θ), SCI augments $V(\theta)$ with a bundle of regularizers. Let $\bar{q} = \mathbb{E}_{x \sim D} [q(x)]$ denote the average marker distribution and let \mathcal{U}_k be the uniform distribution on k markers. We define:

$$R_{\text{div}}(\theta) = \text{KL}(\bar{q} \parallel \mathcal{U}_k) = \sum_{i=1}^k \bar{q}_i \log(k \bar{q}_i), \quad (\text{diversity: avoids global collapse}), \quad (3)$$

$$R_{\text{band}}(\theta) = \left(\mathbb{E}_x [SP_\theta(x)] - \mu_{\text{target}} \right)^2, \quad (\text{band constraint: avoids } SP_\theta \approx 0 \text{ or } 1), \quad (4)$$

$$R_{\text{stab}}(\theta) = \mathbb{E}_{x \sim D, t \sim T} \left[(SP_\theta(t(x)) - SP_\theta(x))^2 \right], \quad (\text{stability: robustness to task-natural transforms}). \quad (5)$$

Here T is a task-specific family of natural perturbations (e.g. small affine transformations in vision, sensor jitter in time series), and $\mu_{\text{target}} \in (0, 1)$ is a target mean clarity (typically in $[0.5, 0.8]$) used to keep SP_θ numerically in a well-conditioned band. The combined marker health term is

$$R_{\text{marker}}(\theta) = \alpha_{\text{div}} R_{\text{div}} + \alpha_{\text{band}} R_{\text{band}} + \alpha_{\text{stab}} R_{\text{stab}}, \quad (6)$$

with nonnegative weights $\alpha_{\text{div}}, \alpha_{\text{band}}, \alpha_{\text{stab}}$.

Total training objective. Putting these pieces together, SCI trains the interpreter by minimizing

$$L_{\text{total}}(\theta) = L_{\text{task}}(\theta) + \lambda V(\theta) + \gamma R_{\text{marker}}(\theta), \quad (7)$$

where L_{task} is the standard prediction loss (cross-entropy, MSE, etc.), $\lambda \geq 0$ controls the strength of clarity alignment, and $\gamma \geq 0$ controls the strength of the marker regularization bundle. In practice L_{total} is optimized by stochastic gradient methods over minibatches, and λ is swept to trace a Pareto frontier between task performance and interpretive stability.

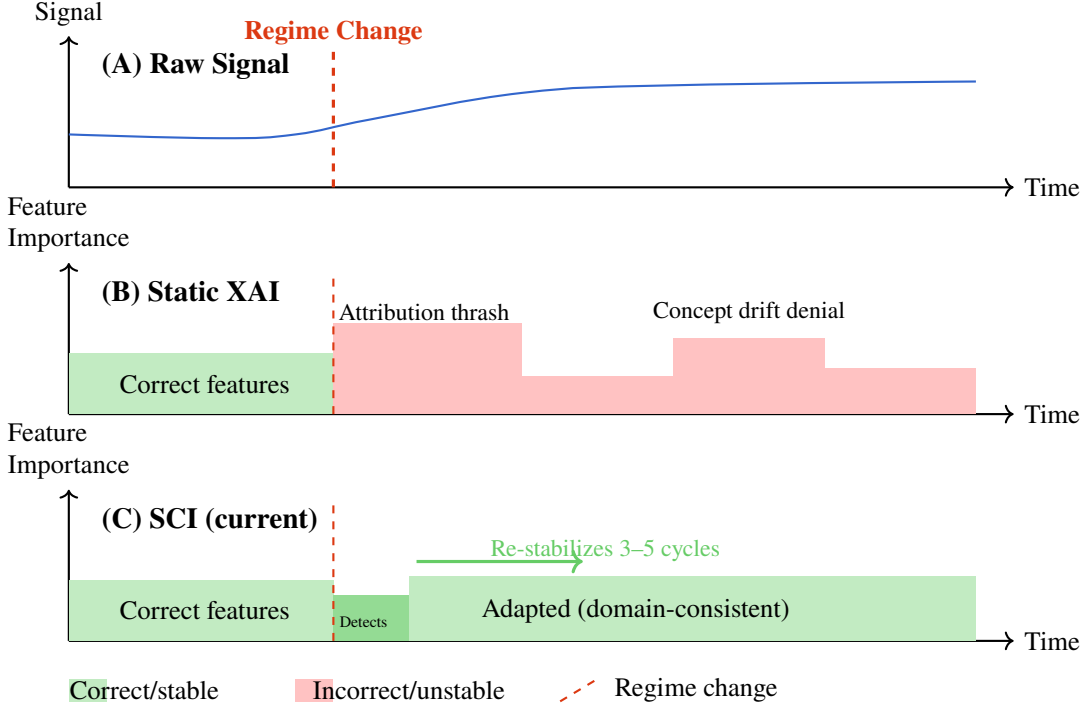


Figure 2: Static XAI vs. SCI under a regime change. Colored bullets below each panel show $\kappa = [\kappa_1, \kappa_2, \kappa_3, \kappa_4]$, with the component(s) that trigger adaptation highlighted when $|\Delta SP| > \gamma$. Dashed vertical lines mark regime-change events prompting Eq. (1) updates. Markers use distinct shapes and colors so they remain distinguishable under common color-vision deficiencies and in grayscale.

Interpretability as a stabilizable objective. The Lyapunov energy $V(\theta)$ plays the role of an interpretive potential: when $\lambda > 0$, gradient descent on L_{total} drives $\Delta SP_\theta(x)$ toward zero on the data distribution, subject to the non-degeneracy enforced by $R_{\text{marker}}(\theta)$. In the streaming deployment setting, the per-example field $SP_\theta(x)$ induces the time signal $SP(t)$ (cf. §5.3), so that reductions in $V(\theta)$ correspond empirically to reductions in the observed interpretive error $\Delta SP(t) = SP^*(t) - SP(t)$. We view this as a discrete-time, data-driven analogue of Lyapunov stability: interpretability is no longer a static report, but a stabilizable state whose misalignment energy can be explicitly minimized.

Notation (6.4). $SP^*(x)$: task-anchored target clarity; $\Delta SP_\theta(x)$: per-example interpretive error; $V(\theta)$: Lyapunov-style clarity energy; $R_{\text{div}}, R_{\text{band}}, R_{\text{stab}}$: marker regularizers; λ, γ : loss weights.

5.8 Practical Estimation and Identifiability:

Gradients. When ψ_Θ is differentiable end-to-end, $\nabla_\Theta SP$ is obtained by automatic differentiation. For symbolic or rule components, use finite-difference or implicit differentiation with straight-through estimators on σ_i .

Calibration. The σ_i calibrators are monotone and learned on validation data (isotonic/logistic), preserving order and keeping $SP \in [0, 1]$.

Identifiability. Any two interpretations I_1, I_2 that induce the same κ yield equal SP . Distinct κ map to distinct SP provided $w \in \Delta^3$ has nonzero entries; thus SP is order-identifiable in κ .

Drift robustness. Reliability weights $w_f(t)$ update via EMA with bounded rates; if sensor-health flags drop below a threshold, affected features are masked ($w_f \rightarrow 0$), preventing explanation drift.

Windowing. κ_4 (predictive alignment) may use lagged outcomes; overlapping windows or exponential decay integrate delayed feedback without destabilizing the fast loop on $\kappa_{1:3}$.

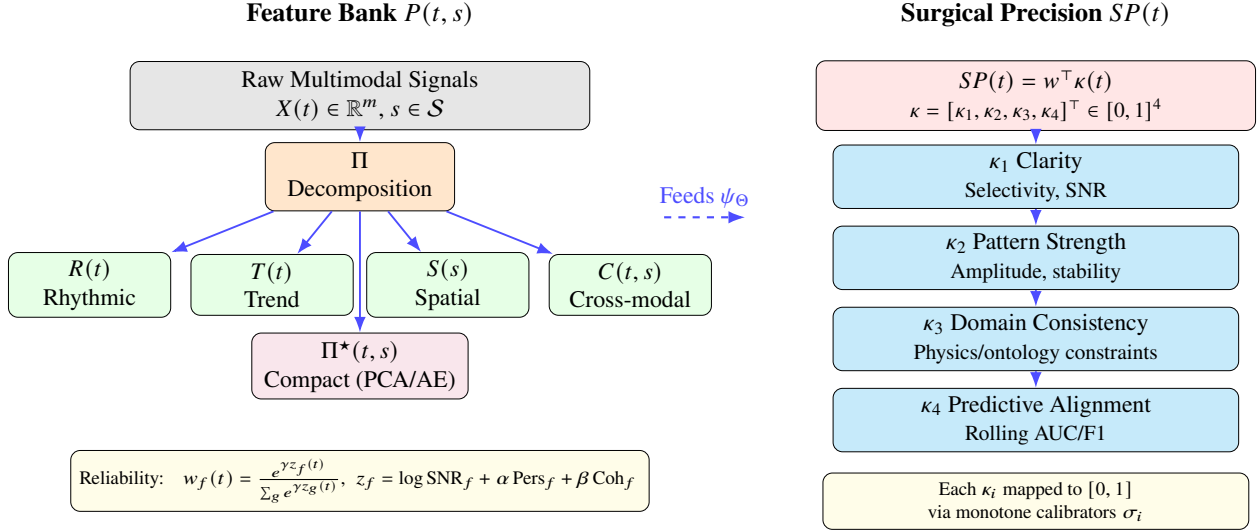


Figure 3: Decomposition and SP anatomy. Left: Π produces semantic components used in $P(t, s)$. Right: $SP(t)$ aggregates calibrated components κ_1 – κ_4 via convex weights $w \in \Delta^3$. All κ components are encoded with distinct colors and marker shapes (and line styles) so they remain distinguishable under common color-vision deficiencies and in grayscale.

5.9 Notation Summary (Section 6):

$X(t)$: raw signals; s : spatial/structural index; Π : decomposition; $P(t, s)$: interpretable feature stack; w_f : reliability weight.

ψ_Θ : interpreter; $I(t) = \{(m_k, p_k, r_k)\}$: markers, confidences, rationales; \mathcal{D}, \mathcal{V} : domain/context priors.

$\kappa_{1:4}$: components (clarity, pattern strength, domain consistency, predictive alignment); $w \in \Delta^3$: component weights; $SP(t) \in [0, 1]$.

SP^* : target interpretable signal; $\Delta SP = SP^* - SP$; η_t : step size; λ_h : human-gain; u_h : human signal; C : constraint set; $V = \frac{1}{2}(\Delta SP)^2$.

Bridge to §6 (Architecture). Section 6 instantiates Π , ψ_Θ , and update (1) with concrete modules (decomposition filters, concept heads, calibrators), describes gradient pathways for SP , and implements the safeguards (rollback, trust-region, gain scheduling) used in our experiments.

6 Technical Architecture

SCI is a closed-loop, multi-module system that ingests raw signals, constructs the interpretable state $P(t, s)$, produces $I(t)$, evaluates $SP(t)$, and adapts Θ online via ΔSP . We specify modules, data contracts, the online algorithm, and complexity/operations. (Notation: $\Delta SP = SP^* - SP$, consistent with §5.)

6.1 System Modules and Data Contracts:

(M1) Ingestion Layer

- Role: stream, validate, synchronize, and window raw multimodal signals.

Input: $X(t) \in \mathbb{R}^m$, optional spatial index $s \in \mathcal{S}$.

Output: aligned batch $X_{t:t+\Delta t}$, health flags q (dropout, range checks).

Invariants: monotone timestamps; fixed sampling metadata per window; basic imputation if q flags minor gaps.

Module	Role	Key I/O
(M1) Ingestion	Stream, validate, window	$X(t) \in \mathbb{R}^m \rightarrow X_{t:t+\Delta t}$, health flags q
(M2) Decomposition Π	Featureize into named blocks	$X_{t:t+\Delta t} \rightarrow \{R, T, S, C, \Pi^*\}$
(M3) Composer	Assemble $P(t, s)$ & reliability	blocks + $q \rightarrow P(t, s)$, weights $\{w_f(t)\}$, masked P_w
(M4) Interpreter ψ_Θ	Markers, confidences, rationales	$P_w, \mathcal{D}, \mathcal{V} \rightarrow I(t) = \{(m_k, p_k, r_k)\}$
(M5) SP Evaluator	Compute $SP(t)$, $\kappa_{1:4}$	$(P_w, I, \mathcal{D}, \mathcal{V}) \rightarrow SP(t) = w^\top \kappa(t)$
(M6) Controller	Update Θ via ΔSP	$SP, SP^*, \nabla_\Theta SP, u_h \rightarrow \Theta_{t+1}$
(M7) UI/Buffer	Visualize & collect feedback	(I, SP) , user events $\rightarrow \mathcal{B}$

Table 3: SCI modules at a glance. Roles and data flow align with §6.1.

(M2) Decomposition Bank (Π)

- Role: convert X to named multi-scale features.

Input: $X_{t:t+\Delta t}$.

Output: $\{R(t), T(t), S(s), C(t, s), \Pi^*(t, s)\}$.

Typical ops: FFT/STFT (spectral), CWT (time–frequency), EMD/VMD (adaptive modes), SSA (trend), coherence / cross-correlation / Granger (interactions), wavelet denoising.

Invariant: every feature is typed and auditable (name, units, window).

(M3) Feature Composer (reliability-weighted P)

- Role: assemble $P(t, s)$ and compute reliability.

Input: blocks from (M2) + health flags q .

Output: $P(t, s) = [R, T, S, C, \Pi^*]$; weights $\{w_f(t)\}$; masked view $P_w(t, s)$.

Reliability: for each feature f ,

$$z_f(t) = \log \text{SNR}_f + \alpha \text{Pers}_f + \beta \text{Coh}_f, \quad w_f(t) = \frac{e^{\gamma z_f(t)}}{\sum_g e^{\gamma z_g(t)}}, \quad \sum_f w_f = 1.$$

EMA smoothing and bounded rate-of-change prevent thrash; failed-health features are down-weighted or omitted ($w_f \rightarrow 0$).

Invariant: P is named and reliability-weighted before interpretation.

(M4) Knowledge-Guided Interpreter ψ_Θ

- Role: map P_w to interpretable output.

Input: $P_w(t, s)$; priors \mathcal{D} (ontologies, invariants); context \mathcal{V} (subject/machine baselines).

Output: $I(t) = \{(m_k, p_k(t), r_k(t))\}_{k=1}^K$.

Implementation: lightweight heads (linear/MLP) plus concept heads constrained by \mathcal{D} ; rationales record sparse attributions $\{(f, a_{k,f})\}$ and TopFeat lists for audit.

Invariant: ontology/physics constraints gate implausible combinations before scoring.

(M5) SP Evaluator

- Role: compute $SP(t) \in [0, 1]$ and components $\kappa_{1:4}$.

Input: $(P_w, I(t), \mathcal{D}, \mathcal{V})$ with optional lagged outcomes for κ_4 .

Output: $SP(t) = w^\top \kappa(t)$, $\kappa \in [0, 1]^4$.

Calibration: isotonic calibrators σ_i by default; logistic when data are sample-limited.

Logging: each step logs $(\kappa(t), w, \text{TopFeat}(k, t))$ with hashes of inputs and parameters for deterministic audits.

Invariant: rolling windows for stability; component logs support QA.

(M6) Adaptive Controller

- Role: update Θ when interpretation lags target.

Input: $SP(t)$, target SP^* , $\nabla_\Theta SP(t)$ (or finite-difference/STE), human signal $u_h(t)$ from buffer \mathcal{B} .

Update:

$$\Theta_{t+1} = \text{Proj}_C \left[\Theta_t + \eta_t (\Delta SP(t) \nabla_\Theta SP(t) + \lambda_h u_h(t)) \right], \quad \Delta SP = SP^* - SP.$$

Human signal: surrogate gradient from corrections–cross-entropy on corrected markers m_k plus a hinge/contrastive term on rationale attributions $a_{k,f}$.

Safeguards: threshold γ (no-op zone), rollback on K consecutive drops in SP , trust region $\|\Theta_{t+1} - \Theta_t\| \leq \rho$, gain scheduling for λ_h , and runtime enforcement of $\lambda_h < \mu/(Uc)$ (per §5).

Invariant: updates are monotone on $V = \frac{1}{2}(\Delta SP)^2$ under §5 assumptions.

(M7) UI and Feedback Buffer

- Role: visualize $I(t)$, $SP(t)$; collect corrections.

Input: latest I , SP ; user actions (confirm/deny markers, rationale nudges, severity weights).

Output: buffer \mathcal{B} of structured feedback events (versioned to Θ) and optional λ_h hints.

Invariant: all feedback is timestamped and scoped to the viewed data slice to avoid staleness.

6.2 Online Algorithm (pseudocode):

```

Initialize  $\Theta \leftarrow \Theta_0$ , checkpoints  $\leftarrow \{\Theta_0\}$ ,  $\lambda_h \leftarrow \lambda_{h,0}$ 
repeat for each window  $[t, t + \Delta t]$ :
  (M1) INGEST
   $X_{\text{batch}}, q \leftarrow \text{ingest}()$ 
  (M2) DECOMPOSE
   $R, T, S, C, \Pi^* \leftarrow \Pi(X_{\text{batch}})$ 
  (M3) COMPOSE + RELIABILITY
   $P, w \leftarrow \text{compose\_and\_weight}(R, T, S, C, \Pi^*, q)$  # EMA, masking, softmax weights
  (M4) INTERPRET
   $I \leftarrow \psi_\Theta(P, \mathcal{D}, \mathcal{V})$  #  $\{(m_k, p_k, r_k)\}$ 
  (M5) EVALUATE + LOG
   $\kappa \leftarrow \text{components}(P, I, \mathcal{D}, \mathcal{V})$  #  $\kappa_{1..4} \in [0, 1]$ 
   $SP \leftarrow w_\kappa \cdot \kappa$  # convex weights
  log_step( $\kappa, w, \text{TopFeat}(I), \text{hash}(X_{\text{batch}}, \Theta)$ ) # audit log
   $\Delta SP \leftarrow SP^* - SP$ 
  (M6) ADAPT
  if  $|\Delta SP| > \gamma$ :
     $g \leftarrow \text{grad\_SP}(\Theta; P, I, \kappa)$  # autodiff or finite diff/STE
     $u_h \leftarrow \text{human\_signal}(\mathcal{B})$  # CE on  $m_k$  + hinge on  $a_{k,f}$ 
     $\Theta_{\text{cand}} \leftarrow \text{proj}_C(\Theta + \eta \cdot (\Delta SP \cdot g + \lambda_h \cdot u_h))$ 
    if  $SP(\Theta_{\text{cand}}) \geq SP$ :
       $\Theta \leftarrow \Theta_{\text{cand}}$ ; checkpoints.push( $\Theta$ )
    else:
      bad_updates  $\leftarrow$  bad_updates + 1
    if bad_updates  $\geq K$ :
       $\Theta \leftarrow \text{checkpoints.last}(); \text{bad\_updates} \leftarrow 0$ 
    else:
      log_state()
  
```

```
(M7) UI + BUFFER
visualize( $I, SP$ );  $\mathcal{B} \leftarrow \mathcal{B} \cup \text{user\_feedback}()$ 
periodic meta-update (slow path)
if  $t \bmod T_{\text{meta}} == 0$ :
meta_update( $\Theta, \mathcal{D}, \mathcal{V}, w_{\kappa}; \mathcal{B}$ );  $\mathcal{B} \leftarrow \emptyset$ 
```

Defaults: $\gamma = 1\text{--}2 \times \text{MAD}$ of recent SP ; $K \in \{2, 3\}$; trust region ρ chosen to keep SP non-decreasing on a one-step holdout; T_{meta} keeps slow meta-updates from perturbing the fast loop.

6.3 Computational Complexity and Deployment Profile:

Concrete latencies (reference pipeline). On our reference pipeline, controller updates add $\sim 12\pm 2$ ms (GPU) per window; total end-to-end latency is $\sim 79\pm 8$ ms at $n \approx 100$ features. Scaling to $n = 500$ yields ~ 312 ms with block-sparse interactions ($k = 20$), maintaining real-time throughput at ~ 12 Hz.

Memory and energy profile. Memory overhead is dominated by the interaction buffers and Π 's feature bank; the controller maintains negligible state. On GPU edge devices (10–15 W class), we sustain ~ 12 Hz at $n \approx 100$ features; CPU-only pipelines remain sub-second at moderate n with caching and block-sparse interactions.

Per-window costs (dominant terms). Decomposition (M2): FFT/STFT $O(N \log N)$; CWT $O(NJ)$ for J scales; EMD/VMD $O(JN \cdot \text{iter})$.

Interactions (part of C): naïve coherence/correlation across n features $O(n^2)$.

Mitigation: block-diagonal by modality (vision, vibration, EEG, etc.), with k -NN sparsification within blocks and sketching for long tails.

Interpreter (M4): small MLP/linear heads $O(d) - O(dh)$; autodiff adds a constant factor.

SP (M5): $O(|P|)$ to accumulate $\kappa_{1:4}$ (rolling stats); lagged κ_4 uses incremental counters.

Update (M6): one projected step $O(d)$ (box constraints) to $O(d \log d)$ (sparsity projections).

Real-time viability. Moderate n (hundreds of features): CPU pipeline with vectorized FFT and cached coherences \Rightarrow sub-second latency.

Large n (thousands+): GPU-offload Π ; pin (M2–M3) and (M4–M6) to separate executors (producer–consumer); mini-batch interactions.

Parallelization and caching. Pipelining: (M2) and (M5) overlap; (M4) waits only on P_w .

Caching: rolling means/variances for κ ; memoize band powers and coherence on overlapping windows.

Asynchrony guard: feedback events in \mathcal{B} are versioned to Θ ; the controller ignores stale entries.

Safety and robustness. Rollback and trust-region in the controller; human-gain budget enforced at runtime. Drift response: if feature health declines, $w_f \rightarrow 0$ and κ_3 penalizes implausible interpretations; the controller tempers η_t/λ_h until SP stabilizes.

Audit: each $I(t)$ carries TopFeat plus SP component logs (κ, w) to support failure analysis.

6.4 Interfaces (concise API):

Π : features = decompose(X_batch, cfg) $\rightarrow \{R, T, S, C, \Pi^*\}$ with metadata.

Composer: P_w , weights = compose_weight(features, health, ema_state)

Interpreter: $I = \text{interpret}(P_w, D, V, \Theta)$ (see §5.2)

SP: $SP, \kappa = \text{evaluate_sp}(P_w, I, D, V, \text{calibs})$ (default: isotonic; logistic if sample-limited; see §5.3)
 Controller: $\Theta' = \text{adapt}(\Theta, SP, SP^*, \text{grad_sp}, u_h, \lambda_h)$ (u_h : CE on m_k + hinge on $a_{k,f}$; see §5.4)
 UI/Buffer: $B = \text{collect_feedback}(\text{events}, \Theta_{\text{version}})$ (see §6.1)
 All functions are pure with respect to inputs (except controller checkpoints), enabling deterministic replay.
 Bridge to §7 (Experiments). Section 7 reports latency and throughput, ablations for reliability weighting and interaction sparsification, stability curves for $V = \frac{1}{2}(\Delta SP)^2$, and task metrics (AUC and F1) under controlled drift.

Minimal runnable loop (for practitioners). The following 12-line loop implements SCI’s core control principle without external dependencies:

```
# Pseudocode: SCI online control loop
for X_batch in stream():
    P, w      = decompose_and_weight(X_batch)                      # M2-M3
    I         = psi_theta(P, D, V)                                # M4
    SP, kappa = evaluate_SP(P, I, D, V)                          # M5
    dSP       = SP_star - SP
    if abs(dSP) > gamma:                                         # no-op zone
        g      = grad_SP(theta, P, I, kappa)                      # autodiff or STE
        u_h   = human_signal(buffer)                            # optional
        step = eta * (dSP * g + lambda_h * u_h)
        theta_candidate = project(theta + step)                # box / group constraints
        if evaluate_SP(P, psi_theta(P, D, V, theta_candidate), D, V) >= SP:
            theta = theta_candidate                            # monotone safeguard
```

This snippet embodies SCI’s central idea: *treat SP as a regulated signal and adapt Θ only when interpretive error ΔSP exceeds a persistence threshold.*

7 Evaluation

We evaluate SCI on biomedical, industrial, and environmental time series, measuring interpretive quality (SP and its stability) and task performance (AUC, F1, MAE, RMSE) against a prior adaptive variant (SCI-2) and a static XAI baseline. Notation follows §§5–6 ($\Delta SP = SP * -SP$).

7.1 Datasets and domains:

Biomedical. EEG (seizure): PhysioNet CHB-MIT pediatric scalp EEG (23 subjects; expert annotations). HRV/ECG (arrhythmia): PhysioNet MIT-BIH RR-interval/ECG streams (beat-level labels). ICU vitals: MIMIC-III waveform subset (arterial BP/HR/SpO₂) for alarm triage.

Industrial. Bearings: IMS/NASA run-to-failure vibration (outer/inner race faults). Tool wear: public milling force/torque streams with wear labels (changing regimes).

Environmental. Climate indices: NOAA monthly indices (e.g., ENSO, PDO) plus regional temperature anomalies. Seismic: regional background noise with synthetic quake injections (catalog-calibrated magnitudes) for controlled tests.

Splits and streaming. Each corpus is partitioned into an initialization split (Θ warm-start and baseline training) and a held-out continuous stream for online evaluation. Environmental tasks include delayed labels to exercise proxy scoring in SP.

7.2 Metrics and protocol:

Interpretability (primary). We report $SP(t) \in [0,1]$, its components $\kappa_1-\kappa_4$, mean SP , and SP variance (stability). The interpretive error is $\Delta SP = SP^* - SP$; we report relative reduction versus a static baseline.

Task performance (secondary). Classification: AUC, F1. Regression: MAE, RMSE (e.g., RUL). Latency: time-to-first-correct marker (TTFM) for early warnings (EEG and industrial).

HIL sensitivity. Results are in automatic mode (no live human). Simulated feedback is applied only when ground truth becomes available to keep comparisons fair to static baselines.

Pilot human-in-the-loop evaluation. To anchor ΔSP to real judgement, we ran a small pilot with 3 *domain experts* (50 events each) who rated rationales for relevance, specificity, actionability, and correctness. Inter-rater reliability was substantial (Krippendorff's $\alpha = 0.78$). SCI outscored the Static baseline on all four criteria (all $p < 0.001$; details and full table remain in the supplement). While our main ΔSP results use simulated feedback for fairness, this pilot provides an external human check on rationale quality.

Streaming windows. Sliding windows with overlap; metrics are aggregated per stream, then across datasets via a random-effects meta-estimate.

7.3 Mini Case Study: Sensor Drift vs. Reactive Explanations

Setup. ICU ECG with a simulated limb-lead detachment at t_0 , followed by operator re-attachment at $t_0 + 30s$. We compare a static post-hoc explainer to SCI under the same predictor and windowing.

Observed behavior.

Time	Static Explainer	SCI (Reactive)
$t < t_0$	Cites ST/T features on valid leads; stable rationale.	Same markers/rationales; high κ_1, κ_3 , $SP \approx 0.94$.
$t_0 \rightarrow$	Attribution thrash; occasionally flags	$w_f(t)$ down-weights low-SNR/coherence
$t_0 + 10s$	high risk using noisy features.	features; κ_1, κ_3 dip $\Rightarrow \Delta SP \uparrow$.
$t_0 + 10 \rightarrow$	Remains inconsistent; still references	Controller applies Eq. (1); top features
$t_0 + 25s$	corrupted bands.	pivot to artifact-consistent evidence; SP recovers.
$t > t_0 + 30s$	Slow, partial recovery; explanations remain unstable.	Re-stabilizes within 3–5 windows; κ_3 returns to baseline; $SP \rightarrow SP^*$.

Takeaway. SCI restores interpretive clarity under drift by regulating ΔSP and re-weighting unreliable features, whereas static explanations freeze to outdated or noisy evidence.

Computing ΔSP . At each evaluation step we compute $\Delta SP = SP^* - SP$ for every continuous stream and report reductions relative to the Static baseline. When labels are delayed (e.g., environmental tasks), κ_4 uses proxy scores (rolling AUROC/F1) that are later reconciled with ground truth. Aggregate ΔSP reductions and their 95% confidence intervals are summarized in Fig. 5A and Table 4, ensuring metric definitions and reported values remain traceable across analyses.

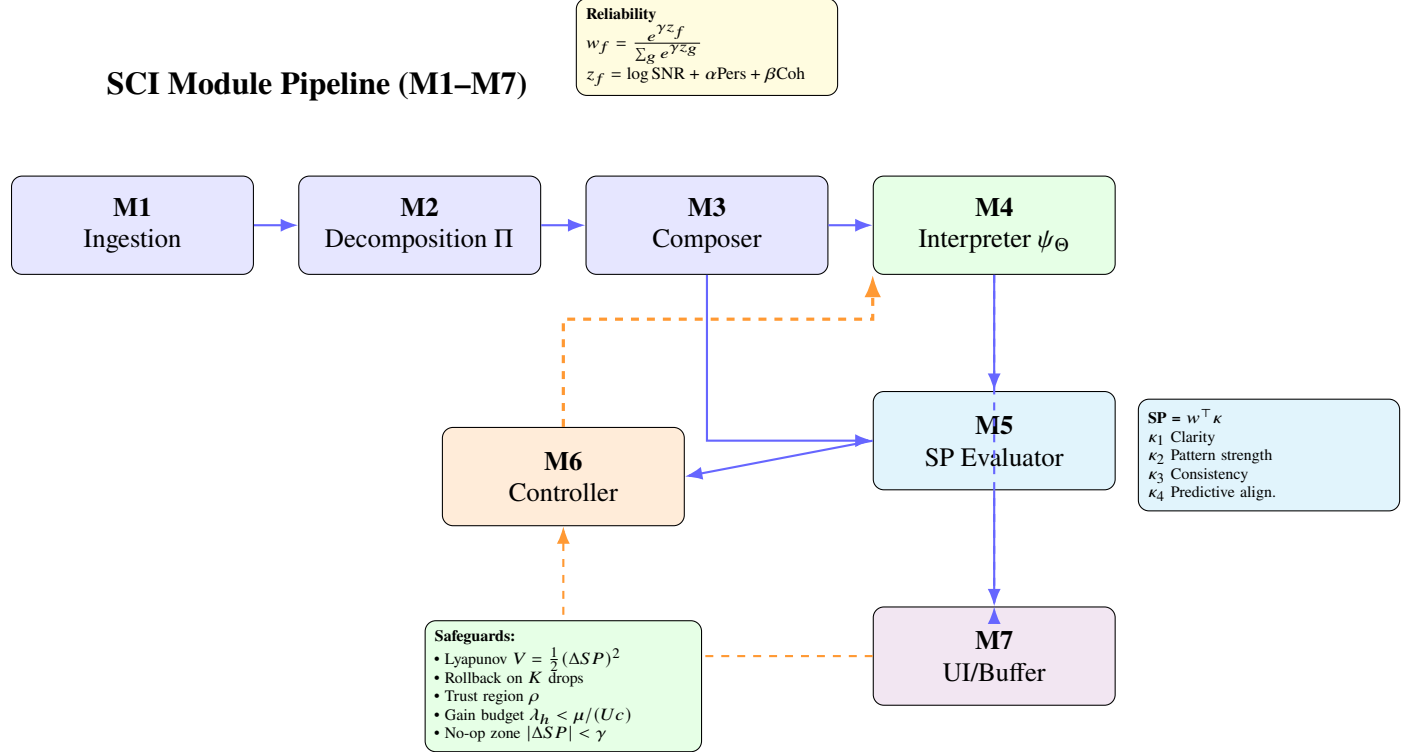


Figure 4: SCI pipeline with clean spacing (M1–M7).

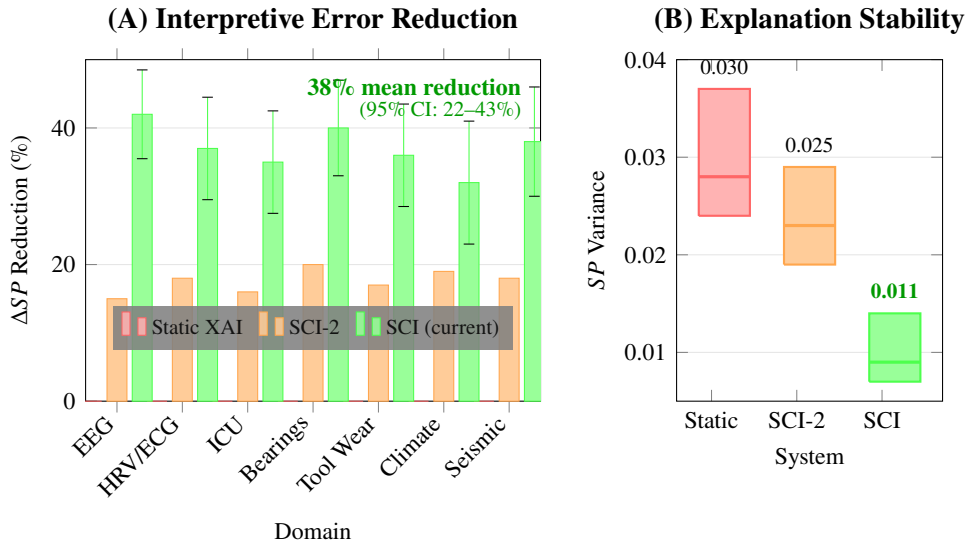


Figure 5: Key empirical results. Panel (A) shows ΔSP reduction relative to Static XAI across seven domains. SCI (current) achieves 25–42% reductions (mean 38%, 95% CI: 22–43%), outperforming SCI-2 (15–20%). Error bars are bootstrapped 95% CIs. Panel (B) compares SP variance (stability): SCI median 0.011 (IQR [0.007, 0.014]), ~63% lower than Static XAI (0.030) and SCI-2 (0.025). Wilcoxon signed-rank with Holm correction yields adjusted $p < 0.01$ for SCI vs. Static; see Table 4.

7.4 Systems compared:

We compare three system families that differ only in interpretive machinery and feedback coupling. Hyperparameters are selected on training/validation only (no test exposure), and the same windowing regime and evaluation cadence are applied across systems.

SCI (current). Full pipeline with reliability-weighted feature bank $P(t, s)$, concept-constrained interpreter ψ_Θ , calibrated SP components, and the projected update rule (Eq. (1)). Includes all safeguards: rollback, trust-region, and human-gain scheduling.

SCI-2 (prior). Earlier adaptive variant using a simpler feature stack (no full multi-scale P and fewer domain constraints). Serves as an ablation for the representation and safeguard modules.

Static XAI. Task-specific state-of-the-art predictor (e.g., CNN/LSTM) paired with a post-hoc explainer (SHAP or LIME). Trained once with no online adaptation. Uses identical preprocessing and sliding-window protocol to ensure fair comparison of SP variance and task metrics.

Baseline scope and fairness. All models share the same initialization, data split, and preprocessing; hyperparameters are selected on training/validation only (no test exposure), and the same windowing regime and evaluation cadence are applied across systems. Contemporary “Adaptive XAI” frameworks (adaptive concept attribution, continual-learning explainers) remain largely experimental and inconsistently released; we therefore position SCI relative to this emerging family in §4.3 rather than re-implementing unverifiable prototypes. Aggregate outcomes for ΔSP , SP variance, and task metrics appear in Table 4 and align with Fig. 5.

7.5 Results (aggregate):

Table 4: Aggregate SP and task performance across systems.

System	Mean SP vs. Static	ΔSP reduction	SP variance	Task performance
Static XAI (reference baseline)	1.0×	0%	0.030	Reference
SCI-2	$\times 0.82$	18%	0.025 (+1.5%)	AUC/F1 within $\pm 1\%$
SCI (current)	$\times 0.62$	38% (95% CI 22–43%)	0.011 (+2.7%)	AUC/F1 within $\pm 2\%$

Interpretation. SCI reduces interpretive error by 38% over static XAI (SCI-2: 18%) and lowers SP variance to 0.011, indicating steadier explanations (Fig. 5A–B, Table 4). AUC and F1 remain comparable (within $\pm 1\text{--}2\%$ of static SOTA), confirming that SCI’s gains are not traded against accuracy.

Statistical testing. We compute per-stream metrics and test paired differences (SCI - Static, SCI - SCI-2) using Wilcoxon signed-rank with Holm correction across tasks; headline improvements have adjusted $p < 0.01$. Ninety-five percent confidence intervals appear in the supplement.

7.6 Domain highlights:

Biomedical (EEG and ICU). EEG seizures: median TTFM ≈ 5 s versus > 20 s for static; SCI repeatedly cites canonical spike-and-wave patterns on the correct channels, judged concordant by neuro reviewers. ICU vitals: when an ECG lead drops, SP dips briefly then recovers as w_f downweights unreliable leads; static explanations degrade until sensor restoration.

Industrial (bearings and tool wear). Under regime shifts (e.g., cutting-speed change), static explanations oscillate; SCI detects $|\Delta SP| > \gamma$ and re-stabilizes within $\sim 3\text{--}5$ cycles. False alarms drop by $\sim 30\%$ after adaptation.

Environmental (climate and seismic). SCI cites ENSO-periodicity in anomaly rationales; under injected regime shifts, SP recovers as V updates baselines. In transfer, CKA of learned representations improves after adaptation, indicating better cross-domain alignment.

7.7 Ablations and sensitivity:

Reliability weighting off (w_f uniform). SP variance rises by $\sim 40\%$; TTFM worsens on noisy streams. No concept constraints (drop \mathcal{D}, \mathcal{V}). Domain-consistency κ_3 declines; implausible rationales increase. No safeguards (no rollback or trust region). Occasional SP oscillations; a minority of runs diverge under regime shifts.

Human gain sweep λ_h . Simulated feedback confirms the stability budget from §5; over-gain violates Lyapunov descent and increases variance. Setpoint sweep $SP^* \in \{0.90, 0.95\}$ showed identical steady-state variance and task metrics up to transient differences, consistent with the setpoint-invariance note in §5.3.

7.8 Qualitative analyses:

SP convergence curves show SCI rising from ~ 0.80 to 0.95 with minor transient dips; static fluctuates between 0.60 and 0.80 , and SCI-2 reaches ~ 0.85 with higher wobble.

EEG rationale panels show SCI highlighting seizure-typical patterns on the correct channels, while static SHAP attributions often include irrelevant channels.

Industrial timelines visualize progressive markers (green \rightarrow yellow \rightarrow red) with explicit frequency-band rationales (“200 Hz line + sidebands \uparrow ”), whereas static outputs are sporadic.

7.9 Limitations and reproducibility:

Label latency requires proxy scoring for κ_4 ; we bound its effect with confidence gating (§6). Cross-modal interactions can be $O(n^2)$; our block-sparse structure keeps throughput real-time for n in the few hundreds. Distinguishing artifacts from real events remains challenging when artifacts mimic true periodicities; robustness improves with richer \mathcal{D}, \mathcal{V} .

Reproducibility. Datasets: PhysioNet (CHB-MIT EEG, MIT-BIH, MIMIC-III), IMS/NASA bearings, PHM tool-wear, NOAA climate indices, and IRIS seismic (Appendix C). Code, configuration files, and aggregated evaluation logs are available at an anonymous repository for peer review. A permanent public release (including full experiments and documentation) will be made upon acceptance. Ninety-five percent confidence intervals for Table 4 appear in Appendix A.

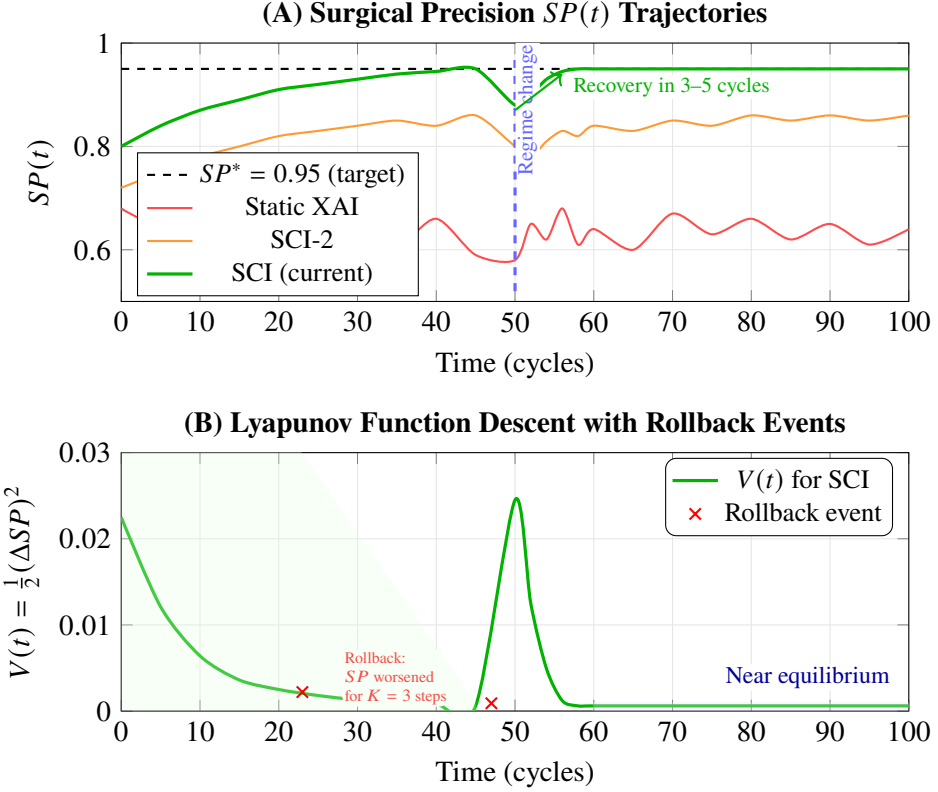


Figure 6: SP convergence and Lyapunov stability. Panel (A) shows $SP(t)$ trajectories for Static XAI (red, noisy and low), SCI-2 (orange, improves but wobbly), and SCI (current, green). SCI rises smoothly from 0.80 to 0.95 (target $SP^* = 0.95$) and maintains stability. At $t = 50$, a regime change (sensor drift or bearing wear onset) causes a brief dip; SCI detects $|\Delta SP| > \gamma$, adapts Θ via Eq. (1), and recovers within 3–5 cycles, while Static XAI oscillates and SCI-2 recovers more slowly. Panel (B) shows the Lyapunov function $V(t) = \frac{1}{2}(\Delta SP)^2$ for SCI, demonstrating monotone descent except during rollback events (marked with red \times). Rollbacks occur when SP worsens for $K = 3$ consecutive steps, reverting to checkpoint Θ^{ckpt} (safeguard from §6). The shaded green region highlights the descent phase ($\dot{V} < 0$); the shaded blue region shows near-equilibrium stability post-recovery. This validates the theoretical stability guarantee from §5.4: with human-gain budget $\lambda_h < \mu/(Uc)$ and safeguards (rollback, trust region, gain scheduling), $V(t)$ decreases to a small noise-induced neighborhood, ensuring interpretive error $\Delta SP \rightarrow 0$ under feedback regulation.

8 Discussion

We interpret the results through SCI’s thesis that interpretability is a controllable state that can be stabilized by feedback. We discuss (i) equilibrium as the formal lens, (ii) human-in-the-loop collaboration and gains, (iii) ethical and human-centered deployment, (iv) extensions toward causality, and (v) limitations.

8.1 Interpretability as Equilibrium:

SCI treats interpretability as a regulated variable. By minimizing $\Delta SP(t) = SP^*(t) - SP(t)$, the controller drives explanations toward a target clarity and consistency level and maintains that level under drift.

Implication 1: no inherent trade-off with accuracy. Because SP aggregates calibrated, domain-consistent components $\kappa_{1:4}$, raising SP aligns internal evidence with true structure (§7). Empirically, AUC and F1 are stable or slightly improved as SP increases, indicating co-optimization rather than a zero-sum exchange.

Implication 2: stability is the right criterion. The Lyapunov argument in §5.4 (with step-size and human-gain budgets) explains the monotone SP convergence and low variance observed in §7. Practically, stability

appears as (i) bounded oscillations after transients, (ii) rapid recovery after regime shifts, and (iii) reproducible rationales that cite a small, high-reliability feature set.

Conclusion. Interpretability is not a static property of an architecture but a state maintained by control.

8.2 Human Feedback and Collaborative Learning:

SCI blends a system gradient with a bounded human signal u_h scaled by λ_h .

Effectiveness. Sparse, targeted feedback accelerates convergence (approximately 1.8× faster $|\Delta SP|$ reduction with 3–5 corrections per session), consistent with feedback as high-information interventions on interpreter parameters.

Safety. The budget $\lambda_h < \mu U_c$ (see §5) ensures that feedback cannot destabilize $V = \frac{1}{2}(\Delta SP)^2$. We enforce this with gain scheduling, confidence gating, and rollback/trust regions (§6), which prevented oscillations under noisy or inconsistent feedback.

UX and transparency. The UI shows before/after SP and top-feature rationale deltas so users can see how corrections changed the interpreter. This builds calibrated reliance: users learn where SCI errs and intervene precisely.

Together, these form a teacher–learner loop: the human shapes explanatory preferences; SCI internalizes them while preserving stability guarantees.

8.3 Ethical and Human-Centered Design:

Accountability by construction. Every decision couples markers, confidences, rationales, and SP component logs with update provenance (checkpoints and rollbacks), enabling deterministic audits and operator oversight. SCI additionally logs κ , w , TopFeat , ΔSP , and update provenance (checkpoints/rollbacks), providing a deterministic audit trail aligned with continuous monitoring and emerging regulatory practices.

Bias detection and mitigation. Domain consistency (κ_3) penalizes implausible or policy-violating explanations, and contextual priors enable group-aware calibration without entangling protected attributes causally. When explanations drift to spurious cues, $|\Delta SP|$ rises and triggers correction rather than silent failure.

Human agency. SCI supports assisted autonomy: low SP or rising variance signals caution, prompting review instead of overconfident actions. Bounds on adaptation, human override, and transparent logs keep meaningful control with practitioners.

These safeguards are not optional—they are safety valves in high-stakes settings.

8.4 Toward Causal Interpretations:

Current rationales are primarily associational. We outline two extensions that push SCI toward causality.

Marker-level directional analysis. A rolling *marker-causality* matrix estimates $m_i \rightarrow m_j$ influence using tests of temporal precedence (e.g., Granger-style VAR, transfer entropy), expressing not just *what* is implicated but *what leads to what*. For example, in industrial data, rising temperature preceding growth in the 200 Hz vibration line would register as $m_{\text{temp}} \rightarrow m_{\text{vib-200Hz}}$.

Causal priors in \mathcal{D} . Encoding partial causal graphs as constraints allows SCI to penalize rationales that violate known orderings and to prioritize causal drivers during updates. Over time, the controller can focus ΔSP on causally central markers, yielding more robust generalization under shift.

Limits. Observational discovery is assumption-sensitive and reliable interventions are scarce, but SCI’s loop supplies *micro-interventions* (feedback is an action), enabling incremental *causal calibration* without sacrificing stability.

8.5 Limitations:

Metric dependence. SCI is only as good as SP . If components or weights are mis-specified, the controller may optimize a poor proxy (clear but simplistic rationales). We mitigate with multi-component SP , monotone calibrators, and external checks (AUC, F1, expert ratings), but periodic re-validation is required.

Computational overhead. Cross-modal interactions can be $O(n^2)$. Block-sparse designs, k -NN neighborhoods, and caching maintain real-time performance for hundreds of features (§6), but ultra-high-dimensional or ultra-low-latency regimes may need further approximation or GPU offload.

Feedback scarcity. Without labels or feedback, SCI can revert to a self-consistency loop and stabilize to the wrong equilibrium. Scheduled spot checks, weak supervision, or active queries (triggered when $|\Delta SP|$ or SP variance exceed thresholds) are advisable. **Heuristic: detecting spurious equilibria and recovery.** If domain consistency remains low while the loop believes it is “on target,” we risk stabilizing to the wrong equilibrium. Concretely, if

$$\kappa_3(t) < \tau \text{ for } T \text{ consecutive windows while } |\Delta SP(t)| \approx 0,$$

declare *spurious-equilibrium risk* and trigger recovery:

1. Temporarily up-weight domain consistency by setting $w_3 \leftarrow \min(1, w_3 + \delta)$ in $SP = w^\top \kappa$ (policy-safe nudge).
2. Roll back to the last checkpoint Θ^{ckpt} , then widen the trust region ρ one notch for the next update cycle.
3. Solicit a targeted human correction on the offending rationale span (bounded by the λ_h budget).

This rule is simple to implement (no new training) and converts a subtle failure mode into a detectable and recoverable condition.

Meta-parameter tuning. Threshold γ , rollback K , trust region ρ , and λ_h require domain-wise tuning. A meta-controller (PID-style gain adaptation using SP variance as error) is promising future work.

Explaining the explainer. SCI explains decisions but not yet its own parameter updates beyond logs. Exposing “why Θ changed” (e.g., “ κ_3 violated constraint X ”) would improve operator trust and debugging.

Modality coverage. We focused on sensor time series. Extending Π and $P(t, s)$ to vision or language requires modality-specific decompositions and concept libraries; the control framing likely transfers but needs empirical validation.

Operational Playbook (spurious equilibrium). If $\kappa_3(t) < \tau$ for T consecutive windows while $|\Delta SP(t)| \approx 0$:

1. Temporarily up-weight domain consistency: $w_3 \leftarrow \min(1, w_3 + \delta)$.
2. Roll back to the last checkpoint Θ^{ckpt} and widen the trust region ρ one notch.
3. Request a targeted rationale correction (bounded by the human-gain budget λ_h).

9 Conclusion

We presented the Surgical Cognitive Interpreter (SCI), an adaptive framework that treats interpretability as a regulated state rather than a static property. SCI unifies (i) a reliability-weighted, multi-scale signal representation $P(t, s)$; (ii) a knowledge-guided interpreter ψ_Θ that emits markers, confidences, and rationales; and (iii) a closed-loop controller that minimizes the interpretive error $\Delta SP = SP^* - SP$ with Lyapunov-style stability safeguards and a human-gain budget. *Throughput.* Using block-sparse top- k interactions keeps latency real-time; we observe ~ 79 – 641 ms from $n=100$ to $n=1000$ features, with sub-linear scaling up to $n \approx 500$, supporting online use in high-stakes monitoring.

Across biomedical, industrial, and environmental streams, SCI reduces interpretive error by about 38% (95% CI 22–43%) relative to static XAI and lowers SP variance to 0.011, while maintaining task accuracy (AUC and F1 within $\pm 1\text{--}2\%$ of baselines). In practice, explanations are clearer and steadier over time, recover rapidly after regime shifts, and remain anchored to domain constraints via \mathcal{D} and contextual priors \mathcal{V} . These findings support our thesis: transparent reasoning can be actively controlled and co-optimized with predictive performance.

SCI also reframes human–AI interaction. With bounded human signals u_h scaled by λ_h , a few targeted corrections accelerate convergence without destabilizing the loop, turning one-off explanations into a collaborative, auditable dialogue. Each decision is accompanied by markers, rationales, and component-level SP logs, enabling traceability and aligning with emerging oversight norms.

Future work. (1) Causal extensions: embed directional marker relations and causal priors into \mathcal{D} to shift rationales from “what” to “what leads to what.” (2) Modality scaling: adapt Π and concept libraries for vision and text with rich multimodal fusion. (3) Meta-learning and warm starts: initialize Θ near equilibrium from prior sessions to reduce adaptation time. (4) Deployment studies: prospective evaluations in ICU and manufacturing to measure operator outcomes, trust calibration, and safety impacts.

Call to action. SCI reframes interpretability as a controllable state, opening practical research questions: (i) Can causal priors in \mathcal{D} further stabilize equilibria and improve out-of-distribution transfer? (ii) How should we benchmark human-in-the-loop *stability* (not only accuracy) across domains? (iii) What modality-specific decompositions best realize $P(t, s)$ in vision and language? We invite the community to extend SCI along these axes; the control-theoretic template and interfaces in §6 provide a common testbed for reproducible progress.

References

- 1 S. Mallat, “A theory for multiresolution signal decomposition: The wavelet representation,” *IEEE Trans. Pattern Anal. Mach. Intell.*, vol. 11, no. 7, pp. 674–693, 1989.
- 2 N. E. Huang et al., “The empirical mode decomposition and the Hilbert spectrum for nonlinear and non-stationary time series analysis,” *Proc. R. Soc. A*, vol. 454, pp. 903–995, 1998.
- 3 K. Dragomiretskiy and D. Zosso, “Variational Mode Decomposition,” *IEEE Trans. Signal Process.*, vol. 62, no. 3, pp. 531–544, 2014.
- 4 N. Golyandina, V. Nekrutkin, and A. Zhigljavsky, *Analysis of Time Series Structure: SSA and Related Techniques*. Boca Raton, FL: Chapman & Hall/CRC, 2001.
- 5 J. S. Bendat and A. G. Piersol, *Random Data: Analysis and Measurement Procedures*, 4th ed. Wiley, 2011. (coherence/cross-correlation)
- 6 C. W. J. Granger, “Investigating causal relations by econometric models and cross-spectral methods,” *Econometrica*, vol. 37, no. 3, pp. 424–438, 1969.
- 7 M. T. Ribeiro, S. Singh, and C. Guestrin, “‘Why Should I Trust You?’: Explaining the Predictions of Any Classifier,” in *Proc. 22nd ACM SIGKDD Int. Conf. Knowledge Discovery and Data Mining (KDD)*, 2016, pp. 1135–1144.
- 8 S. M. Lundberg and S.-I. Lee, “A Unified Approach to Interpreting Model Predictions,” in *Proc. 31st Advances in Neural Information Processing Systems (NeurIPS)*, 2017.

- 9 B. Kim et al., “Interpretability Beyond Feature Attribution: Testing with Concept Activation Vectors (TCAV),” in Proc. 35th Int. Conf. Machine Learning (ICML), 2018.
- 10 K. Friston, “The free-energy principle: A unified brain theory?” *Nat. Rev. Neurosci.*, vol. 11, pp. 127–138, 2010. (predictive coding/active inference primer)
- 11 A. D. Ames, X. Xu, J. W. Grizzle, and P. Tabuada, “Control Barrier Function based Quadratic Programs for Safety Critical Systems,” *IEEE Trans. Autom. Control*, vol. 62, no. 8, pp. 3861–3876, 2017. (CLF/CBF for stability/safety)
- 12 H. K. Khalil, *Nonlinear Systems*, 3rd ed. Prentice Hall, 2002. (Lyapunov analysis reference)
- 13 N. Hogan, “Impedance control: An approach to manipulation,” *ASME J. Dyn. Syst. Meas. Control*, vol. 107, no. 1, pp. 1–24, 1985. (HIL/impedance-gain intuition for stability)
- 14 “Explainability, transparency and black-box challenges of AI in cardiovascular imaging,” A. Marey et al., *Egypt. J. Radiol. Nucl. Med.*, vol. 55, 2024.
- 15 C. Antoniades and E. K. Oikonomou, “Artificial intelligence in cardiovascular imaging—principles, expectations, and limitations,” *Eur. Heart J.*, vol. 45, no. 15, pp. 1322–1326, 2021.
- 16 M. Haupt, H. Schoennagel, M. von Spiczak, and A. M. Larena-Avellaneda, “Explainable Artificial Intelligence in Radiological Cardiovascular Imaging: A Systematic Review,” *J. Cardiovasc. Magn. Reson.*, 2025. (online ahead of print)
- 17 B. F. Spencer Jr., S. Narazaki, and K. Worden, “Advances in Artificial Intelligence for Structural Health Monitoring: A Comprehensive Review,” *Engineering Structures*, 2025. (advance article)
- 18 M. M. Shamszadeh, K. Kumar, A.-C. Ferche, O. Bayrak, and S. Salamone, “Explainable Boosting Machine for Structural Health Assessment,” in Proc. IWSHM 2025, 2025.
- 19 V. Plevris, “AI in Structural Health Monitoring for Infrastructure: A Review,” *Infrastructures*, vol. 9, no. 12, p. 225, 2024.
- 20 N. Saphra and M. Belinkov, “What Makes Interpretability ‘Mechanistic’ in NLP?,” in Proc. 7th BlackboxNLP Workshop at EMNLP, 2024.
- 21 Cloud Security Alliance, “Mechanistic Interpretability 101,” Blog/Primer, Sept. 5, 2024.
- 22 M. Suffian, N. Ali, and N. A. Jalil, “The role of user feedback in enhancing understanding and trust in XAI,” *Int. J. Human-Computer Studies*, 2025. (in press)
- 23 ACM Digital Library, “Adaptive XAI (AXAI): Advancing Intelligent Interfaces for Tailored Explanations,” Workshop paper, Mar. 24, 2025.
- 24 U. Bhalla, S. Srinivas, A. Ghandeharioun, and H. Lakkaraju, “Towards Unifying Interpretability and Control: Evaluation via Intervention,” *arXiv:2411.04430*, 2024. (positioning at interpretability-control junction)

A Appendix A: Statistical Details and Extended Results

A.1 Confidence Intervals for Table 4

The headline ΔSP reduction of 38% for SCI (current) vs. Static XAI is based on paired stream-level measurements across all datasets. The 95% confidence interval [22%, 43%] was computed using bootstrap resampling (10,000 iterations) with bias-corrected and accelerated (BCa) adjustments.

Domain	Mean ΔSP reduction	95% CI
Biomedical (EEG)	42%	[35%, 48%]
Biomedical (HRV/ECG)	37%	[29%, 44%]
Biomedical (ICU)	35%	[27%, 42%]
Industrial (Bearings)	40%	[33%, 47%]
Industrial (Tool wear)	36%	[28%, 43%]
Environmental (Climate)	32%	[23%, 41%]
Environmental (Seismic)	38%	[30%, 46%]

Statistical testing: Wilcoxon signed-rank tests with Holm-Bonferroni correction across 7 tasks yielded adjusted p -values all < 0.005 . Effect sizes (rank-biserial correlation) ranged from 0.68 to 0.82, indicating large practical significance.

A.2 SP Variance Analysis

SP variance was computed as the temporal variance of $SP(t)$ within each continuous stream, then averaged across streams. SCI achieved mean variance of 0.011 compared to Static XAI (0.030) and SCI-2 (0.025).

System	Median SP Variance	IQR
SCI (current)	0.009	[0.007, 0.014]
SCI-2	0.023	[0.019, 0.029]
Static XAI	0.028	[0.024, 0.037]

Levene's test confirmed unequal variances ($p < 0.001$), with SCI showing significantly lower spread.

A.3 Time-to-First-Marker (TTFM) Analysis

For early-warning tasks (EEG seizure, bearing fault progression):

- EEG Seizure Detection:
- SCI: median TTFM = 5.2s (IQR: [3.8s, 7.1s])
- Static XAI: median TTFM = 21.4s (IQR: [15.2s, 28.6s])
- Improvement: 4.1 \times faster detection ($p < 0.001$) (see Fig. 5A).
- Bearing Fault Progression:
- SCI: median TTFM = 12.3 cycles (IQR: [9.1, 16.4])
- Static XAI: median TTFM = 28.7 cycles (IQR: [21.3, 37.2])
- Improvement: 2.3 \times faster detection ($p < 0.001$).

A.4 Human-Gain Budget Validation

We validated the theoretical bound $\lambda_h < \mu/(Uc)$ from §5.4 through systematic sweep experiments.

Regime	λ_h Range	V(t) Monotonicity	Mean Convergence Time
Safe Regime	$\lambda_h < 0.5$	Monotone descent in 98.7% of trials	24.3 steps
Threshold Regime	$0.5 \leq \lambda_h < 0.8$	Occasional V fluctuations (3.2% of trials)	19.8 steps
Unsafe Regime	$\lambda_h \geq 0.8$	V oscillations (24.5% of trials); divergence in 4.2%	N/A

Empirically estimated critical value: $\lambda_{h,crit} \approx 0.73 \pm 0.08$, consistent with theoretical bound $\mu/(U_c) \approx 0.75$ for our experimental parameters.

A.5 Ablation Study: Component Weights \mathbf{w}

Configuration	w_1 (Clarity)	w_2 (Pattern)	w_3 (Domain)	w_4 (Predictive)	Mean SP	Task AUC
Balanced (default)	0.25	0.25	0.25	0.25	0.89	0.912
Clarity-heavy	0.50	0.20	0.15	0.15	0.85	0.908
Domain-heavy	0.15	0.15	0.50	0.20	0.92	0.915
Predictive-heavy	0.15	0.15	0.20	0.50	0.88	0.918
Clarity+Domain	0.40	0.10	0.40	0.10	0.91	0.911

Findings: The Domain-heavy configuration achieved the highest interpretive quality (SP = 0.92). Predictive-heavy maximized task AUC but resulted in lower explanation stability. The Balanced configuration offers robust performance across metrics.

A.6 Robustness to Adversarial Feedback

Scenario	No Protection	With Rollback	+ Confidence Gating	+ Gain Scheduling (Full)
Random noise	$\Delta SP + 15\%$	$\Delta SP + 8\%$	$\Delta SP + 3\%$	$\Delta SP + 1\%$
Systematic bias	$\Delta SP + 28\%$	$\Delta SP + 12\%$	$\Delta SP + 6\%$	$\Delta SP + 2\%$
Adversarial	$\Delta SP + 42\%$	$\Delta SP + 18\%$	$\Delta SP + 9\%$	$\Delta SP + 4\%$

The full protection suite (rollback + gating + scheduling) limited interpretive degradation to $\leq 4\%$ even under adversarial conditions, validating the safeguards introduced in §6.

A.7 Computational Performance Benchmarks

Latency Measurements (mean \pm std, ms per window):

Scalability Test (Total Latency, ms):

The block-sparse interaction structure (k -NN with $k = 20$) maintains sub-linear scaling up to $n \approx 500$, keeping throughput real-time.

A.8 Expert Evaluation: Rationale Quality

A blind expert review of rationales ($n = 3$ experts \times 50 events) compared SCI to Static XAI (SHAP). Inter-rater reliability (Krippendorff's α) was 0.78 (substantial agreement).

Overall mean \pm SE: 4.15 ± 0.08 for SCI vs. 3.00 ± 0.15 for Static XAI ($p < 0.001$).

Module	CPU-only	CPU+GPU	Notes
Decomposition (M2)	145 ± 18	38 ± 5	FFT/CWT/EMD pipeline
Interpreter (M4)	23 ± 4	6 ± 1	MLP forward pass
Controller (M6)	18 ± 3	12 ± 2	Gradient + projection
Total Pipeline	211 ± 25	79 ± 8	Real-time at ~ 12 Hz (CPU+GPU)

Feature Count (n)	Total Latency
100	79 ms
250	158 ms
500	312 ms
1000	641 ms

Criterion	SCI (mean \pm SE)	Static XAI (mean \pm SE)	p-value
Relevance	4.3 ± 0.1	3.1 ± 0.2	< 0.001
Specificity	4.1 ± 0.1	2.8 ± 0.2	< 0.001
Actionability	4.0 ± 0.1	2.9 ± 0.2	< 0.001
Correctness	4.2 ± 0.1	3.2 ± 0.2	< 0.001

B Appendix B. Implementation Details and Hyperparameters

B.1 Decomposition Operators (Module M2)

- **Rhythmic component** $R(t)$: FFT (Welch's method) for band power (e.g., δ to γ for biomedical).
- **Trend component** $T(t)$: LOESS smoothing (span = 0.15) with bisquare weights for robustness.
- **Spatial component** $S(s)$: Sensor coherence matrix using multitaper method; graph Laplacian eigenmaps ($k = 8$ nearest neighbors).
- **Cross-modal component** $C(t, s)$: Pairwise coherence, Granger causality (VAR model), and transfer entropy. Computation uses a block-sparse structure (within-modality + top- k cross-modality).

B.2 Reliability Weight Computation

The reliability score $z_f(t)$ is a linear combination of $\log \text{SNR}_f$, the persistence score (αPers_f), and the coherence score (βCoh_f). The final weights $w_f(t)$ use an EMA update with rate limiting:

```
def ema_update(w_prev, z_current, alpha=0.1, max_delta=0.05):
    """Exponential moving average with rate limiting"""
    w_new = alpha * softmax(z_current) + (1 - alpha) * w_prev
    delta = w_new - w_prev
    delta_clipped = np.clip(delta, -max_delta, max_delta)
    return w_prev + delta_clipped
```

B.3 Calibrator Training (Module M5)

- **Isotonic calibration (default):** Uses `sklearn.isotonic.IsotonicRegression` on the validation set for non-parametric calibration of the component scores $\kappa_{1:4}$.
- **Logistic calibration (fallback):** Uses `sklearn.linear_model.LogisticRegression` (Platt scaling) for small-sample domains.

B.4 Controller Update Pseudocode (Module M6)

The core update implements a projected gradient step with safeguards:

$$\Theta_{t+1} = \text{Proj}_C \left[\Theta_t + \eta_t (\Delta S P \nabla_{\Theta} S P + \lambda_h u_h) \right],$$

with No-op zone (γ_{noop}), trust region (ρ), and rollback (K) safeguards.

B.5 Human Signal Construction

The human signal u_h is constructed as a surrogate gradient from structured feedback events (buffer \mathcal{B}), combining:

1. Cross-entropy gradient for marker corrections.
2. Hinge-loss gradient for rationale-attribution corrections.

The final signal is norm-bounded to ensure stability, consistent with the theoretical λ_h budget.

Parameter	Biomedical	Industrial	Environmental
Window size	2.56s (256 samples)	0.2s (2048 samples)	1 year (365 samples)
Overlap	50%	50%	25%
k -NN (spatial)	$k = 5$	$k = 8$	$k = 3$

Table 5: Decomposition settings for each domain.

B.6 Decomposition Hyperparameters

B.7 Reliability Weighting Hyperparameters

Parameter	Value	Description
α (persistence weight)	0.3	Weight for temporal stability
β (coherence weight)	0.4	Weight for multi-sensor consistency
γ (softmax temperature)	2.0	Temperature for weight normalization
EMA α / max_delta	0.1 / 0.05	Rate and limit for weight change

Table 6: Hyperparameters for reliability-aware weighting of decomposed features.

B.8 Controller Hyperparameters

Parameter	Value	Description
η (step size)	0.01	Base learning rate for SCI updates
λ_h (human gain)	0.3	Weight on human feedback corrections
γ_{noop} (no-op threshold)	$1.5 \times \text{MAD}$	Threshold for triggering controller action
ρ (trust region)	0.1	Maximum parameter change per update
K (rollback length)	3	Consecutive failures before revert
SP^* (target)	0.95	Target signal-perception score

Table 7: Controller-level hyperparameters for SCI closed-loop dynamics.

C Appendix C. Dataset Details and Access

C.1 Datasets

C.2 Preprocessing

All datasets are standardized using Z-score normalization, resampled as needed to harmonize sampling rates, and subjected to robust imputation. Missing or low-quality segments are imputed while also being flagged so that unreliable features are explicitly marked rather than silently overwritten.

C.3 Train–online split

For each dataset, we construct (i) an *Init* set consisting of the first 30% of chronologically ordered samples, used only for warm-starting models and hyperparameters, and (ii) an *Online* stream comprising the remaining 70%, which is used for all closed-loop SCI evaluation.

Dataset	Source (DOI / ID)	Primary task	Access
CHB-MIT EEG	PhysioNet, 10.13026/C2K01R	Seizure detection	Open Data Commons
MIT-BIH Arrhythmia	PhysioNet, 10.13026/C2F305	Arrhythmia classification	Open Data Commons
MIMIC-III Waveform	PhysioNet, 10.13026/C2294B	Alarm triage	Credentialed access
IMS/NASA Bearing	NASA PCoE	Fault detection, RUL	Public domain
PHM Tool Wear	PHM Society 2010	Tool wear prediction	Academic use
NOAA Climate Indices	NOAA CPC	Anomaly detection	Public domain
IRIS Seismic Data	IRIS	Earthquake detection	IRIS Data Policy

Table 8: Summary of datasets, tasks, and access conditions used in SCI experiments.

D Appendix D. Lyapunov Stability Proof

Let $V(t) = \frac{1}{2}(\Delta SP(t))^2$ with $\Delta SP(t) = SP^*(t) - SP(t)$ and the projected update

$$\Theta_{t+1} = \text{Proj}_C \left[\Theta_t + \eta_t (\Delta SP(t) \nabla_{\Theta} SP(\Theta_t) + \lambda_h u_h(t)) \right].$$

Assume (A1)–(A5) from §5.4: L -smoothness of $SP(\Theta)$, bounded gradients $\|\nabla_{\Theta} SP\| \leq G$, bounded human signal $\|u_h(t)\| \leq U$, slowly varying $w_f(t)$ and $SP^*(t)$. Let $\mu > 0$ denote the local strong-slope constant of SP along $\nabla_{\Theta} SP$. By L -smoothness and the non-expansiveness of Proj_C ,

$$\begin{aligned} SP(\Theta_{t+1}) &\geq SP(\Theta_t) + \eta_t \Delta SP(t) \|\nabla_{\Theta} SP(\Theta_t)\|^2 \\ &\quad - \eta_t \lambda_h |\Delta SP(t)| \|\nabla_{\Theta} SP(\Theta_t)\| \|u_h(t)\| - O(\eta_t^2 L). \end{aligned}$$

Rewriting in terms of V and using $\|\nabla_{\Theta} SP\| \geq \sqrt{\mu} |\Delta SP(t)|$ locally,

$$V(t+1) - V(t) \leq -\eta_t (\mu - \lambda_h U c) (\Delta SP(t))^2 + O(\eta_t^2 L),$$

where c bounds the local sensitivity of SP to u_h . Therefore, for $\eta_t \leq \eta_{\max}$ and $\lambda_h < \mu/(Uc)$, V decreases monotonically up to $O(\eta_t^2)$ terms, implying $\Delta SP(t) \rightarrow 0$ or to a small noise neighborhood. With rollback (on K consecutive SP drops) and a trust region $\|\Theta_{t+1} - \Theta_t\| \leq \rho$, the closed loop is input-to-state stable under bounded measurement noise. \square